NASA TECHNICAL NOTE

NASA TN D-4171

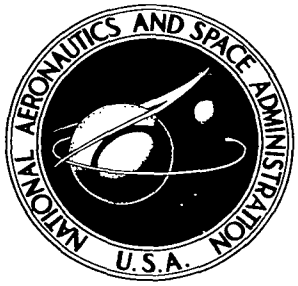

NASA TN D-4171

NORMAL GRAVITY SELF-PRESSURIZATION OF 9-INCH- (23 CM) DIAMETER SPHERICAL LIQUID HYDROGEN TANKAGE

by John C. Aydelott

Lewis Research Center
Cleveland, Ohio

NATIONAL AERONAUTICS AND SPACE ADMINISTRATION • WASHINGTON, D. C. • OCTOBER 1967

NASA TN D-4171

NORMAL GRAVITY SELF-PRESSURIZATION OF 9-INCH- (23 CM) DIAMETER SPHERICAL LIQUID HYDROGEN TANKAGE

By John C. Aydelott

Lewis Research Center
Cleveland, Ohio

NATIONAL AERONAUTICS AND SPACE ADMINISTRATION

For sale by the Clearinghouse for Federal Scientific and Technical Information
Springfield, Virginia 22151 – CFSTI price $3.00

NORMAL GRAVITY SELF-PRESSURIZATION OF 9-INCH- (23 CM) DIAMETER SPHERICAL LIQUID HYDROGEN TANKAGE

by John C. Aydelott

Lewis Research Center

SUMMARY

A nonventing 9-inch- (23 cm) diameter spherical container partially filled with liquid hydrogen was subjected to 21 quiescent self-pressurization tests. The hydrogen container was subjected to various combinations of the variables percent filling, heat-transfer rate, and either top heating, bottom heating, or uniform heating. The pressure-rise rate in the hydrogen container was primarily a function of the heating configuration with the percent filling and heat-transfer rate playing a secondary role. An analysis is presented for determining the resulting energy distribution within the hydrogen container. Appreciable energy transfer from the vapor to the liquid causing evaporation and liquid heating occurred during both the uniform heating and top heating tests.

INTRODUCTION

The NASA space exploration program is heavily dependent on the use of liquid hydrogen as a rocket fuel. Liquid hydrogen has many properties, in addition to a very low boiling point, which set it apart from common liquids. Of particular interest are the thermal transport properties of both liquid and gaseous hydrogen which make it possible for subcooled liquid and highly superheated vapor to coexist in the same container. This situation occurs when a closed system containing liquid hydrogen is exposed to energy input in the form of heat which causes an increase in the total system pressure. The interface between the liquid and vapor phases remains at the saturation temperature corresponding to the increasing vapor static pressure, or total pressure. The average liquid temperature increases at a slower rate and thus the liquid becomes subcooled; the average vapor temperature increases at a faster rate and thus the vapor becomes superheated. As a consequence, simple thermodynamic analysis cannot predict the rate of pressure rise in a closed system containing liquid hydrogen.

An excellent review of the work that has been performed in this field will be found in reference 1. The majority of the reported work has been restricted to cylindrical tanks with heating only on the side walls so that natural convection theory for vertical plates could be used to predict the heat and mass transfer within the liquid phase. In general, direct heating of the vapor was not considered. For the present study both the geometry of the hydrogen container and the basic heat-transfer mechanisms were different. Consequently, no attempt was made to correlate the resulting data with existing analyses and no detailed discussion of earlier work is included.

This report presents the information obtained from 23 self-pressurization tests of spherical tanks containing liquid hydrogen. Twenty-one of the tests were performed with the experiment rigidly held so that the liquid-hydrogen interface was quiescent. Two tests involved violent shaking of the experiment in order to obtain a saturated homogeneous mixture of hydrogen liquid and vapor.

The purpose of the quiescent tests was to compare and explain the differences in the pressure-rise rate in a spherical hydrogen container as a function of heat-transfer rate, heat-flux distribution, and percent filling of the container. The homogeneous tests were used for calibration of the temperature transducers and error analysis.

The experiment consisted of a 9-inch- (23 cm) diameter vacuum-jacketed spherical container partially filled with liquid hydrogen. A thin wall, 0.010 inch thick (0.0254 cm), hydrogen container was used to simulate a flight-weight vehicle. The hydrogen container was surrounded by two hemispherical radiant heaters whose temperatures could be controlled in order to vary the distribution and rate of energy input to the hydrogen container. The maximum heat-transfer rate employed was equivalent to the rate of energy absorbed by a bare stainless-steel tank in space exposed to the Sun.

ANALYSIS

Thermodynamic Pressure Rise

The first law of thermodynamics is

$$Q = \Delta U + \int P \, dV$$

(Symbols defined in appendix A.) For a closed, nonexpanding system, all the heat absorbed by the system manifests itself in a change in the total internal energy of the system; that is, for $dV = 0$

$$Q = \Delta U$$

If the system in question is a tank containing a liquid and its vapor, a knowledge of how the added heat affects the internal energy distribution, and thus the temperature distribution within the tank, makes prediction of the total system pressure possible. For a two-phase mixture, temperature and pressure are dependent variables at the interface between the liquid and the vapor.

The temperature distribution in a cryogenic storage tank is highly complex and is affected by many variables, the most important of which are tank geometry, percent filling, heat-flux rate, and heat-flux distribution.

This report presents two simple pressure rise models that are not intended to be attempts at describing the process that actually takes place in a nonventing hydrogen container but are intended to be a means of comparing one set of experimental data with another. The position that experimental data assume in relation to the theoretical models on a plot of total pressure against heat added is then a qualitative indication of how the energy is being distributed within the hydrogen container. The first model assumes homogeneous conditions (uniform temperature) throughout the hydrogen container and is a common calculation that is performed to compare data of this type. The second model assumes that all the energy absorbed by the hydrogen container goes into the evaporation of liquid and maintaining the vapor at the saturation temperature corresponding to total system pressure. The liquid-phase temperature remains constant at the saturation temperature corresponding to seal-off pressure.

Figure 1 is a theoretical plot of tank pressure as a function of heat added for the two energy distribution models. The plot is for 1 cubic foot (0.02832 cu m) container and initial liquid fillings of 25, 50, and 75 percent by volume. The reader may approximate the energy input, as determined by these models, that will cause a specified change in pressure for any tank size or filling. This is possible by interpolating to determine the effect of percent filling and by multiplying the heat added by the volume of the tank in cubic feet since the energy input is a linear function of the tank volume. Appendix B contains the development of the theoretical models based on the first law of thermodynamics.

Heat Transfer

In order to obtain the energy input to a real tank a heat-transfer analysis must be performed. Appendix C contains the details of the heat-transfer analysis used for this experimental program. The main source of energy input to the experiment was radiant exchange from the heaters. Conduction along the plastic support ring, vent tube, and instrumentation wires played a secondary role. The resulting heat-transfer rates are based on the area of the inner sphere.

Energy Distribution

Once the total energy input to the liquid-hydrogen tank is known, it is of interest to know how the energy input effects the contents of the tank; namely, how much of the total energy input goes into heating the vapor, evaporation of liquid, or heating the liquid. At any time during the test the temperature distribution in the vapor and the pressure can be determined from the instrumentation. This makes it possible for the internal energy and mass of the vapor to be calculated at any time, and thus the energy which went into heating vapor and evaporation, mass change times heat of vaporization, during the time interval of interest can be determined. The energy input to the liquid during the same time interval can then be found by subtracting the energy which went into the vapor and evaporization from the total input during the time period. From knowledge of the change in the temperature of the bulk of the liquid and the fact that the interface between the liquid and the vapor remains at the saturation temperature, the energy input to the liquid can be further broken down into the energy that goes into heating the bulk of the liquid and that which heats the layer of fluid between the bulk and the liquid-vapor interface. A detailed development of this analysis will be found in appendix D.

APPARATUS

Liquid Hydrogen Container

Figure 2 is a cross-sectional drawing of the liquid-hydrogen experiment that consisted of three concentric spheres; the inner sphere contained the liquid hydrogen, the intermediate sphere had electric heating coils mounted on its exterior surface, and the outer sphere served as a vacuum jacket to reduce the gaseous conduction of heat. The vacuum jacket had coils mounted on its exterior surface through which liquid nitrogen was circulated during each test in order to minimize the conduction heat transfer to the inner sphere. The inner sphere and the inner surface of the heaters were painted black in order to increase their emissivity. The vent tube was made of stainless steel. The inner sphere was supported by the vent tube and a polychlorotrifluoroethylene plastic ring that was cut out where possible to reduce heat conduction.

A heater controller, which basically consisted of a bridge circuit which balanced the resistance of a temperature sensor on each heater with a corresponding rheostat on the control panel, was used to maintain heater temperatures of 360°, 425°, 500°, or 575° R (200°, 236°, 278°, or 319° K).

Instrumentation

Temperature and pressure transducers measured the total system pressure, vacuum-space pressure, surface temperatures of the inner sphere, heater, and vacuum jacket, and temperature at 17 locations inside the inner sphere. Figure 3 shows the location of the temperature transducers on the inner sphere and the four carbon resistor temperature rakes that were located within the inner sphere to measure the temperature of the hydrogen liquid and vapor. Figure 4 is a photograph showing two of the carbon resistor rakes. At any time prior to a test run the resistance of any temperature transducer could be determined by the use of a digital ohmmeter mounted in the control panel. During a test the resistance of each transducer was measured by using two bridges and amplifiers so that temperature changes were converted to 0- to 5-volt signals which were recorded on magnetic tape. For each transducer one bridge had a 0- to 5-volt range corresponding to anticipated changes in liquid temperature and the second bridge had a 0- to 5-volt range corresponding to the much larger anticipated changes in vapor temperature.

A very small electric current is passed through a temperature transducer to determine the resistance and thus temperature of the transducer. When a relatively high current is applied to a carbon resistor, its temperature is quite different depending on whether the temperature probe is in the liquid or vapor phase. This is due to self-heating. Exploitation of this fact, together with careful arrangement of the carbon resistors, makes it possible to use the carbon resistors to determine the liquid level in the sphere prior to the start of a test.

Temperature transducers were located on the intermediate and outer spheres so that the heat transfer to the inner sphere by radiation and conduction could be calculated. A single-bridge recording system similar to the one used for the inner-sphere temperature transducers was employed.

An ionization gage was used to measure the pressure in the vacuum space. The location of the gage and the attachment point of the two pressure transducers used to measure the pressure in the inner sphere can be seen in figure 2. A 28-volt direct-current power supply was used to operate the pressure transducers. The vacuum pressure was monitored continuously on the control panel. During a test the 0- to 5-volt output of the inner-sphere pressure transducers was recorded on magnetic tape.

PROCEDURE

Prior to the assembly of the experiment, thermocouples were attached to the inner sphere, heaters, and vacuum jacket. All temperature transducers were calibrated at

139.5° R (78° K) by submerging the three spheres in a liquid nitrogen bath. The inner sphere, heaters, and vacuum jacket were calibrated in a carefully controlled oven at 540° R (300° K). In addition, the heater temperature transducers were calibrated at 710° R (394° K) in the oven. After the experiment had been assembled it was filled with liquid hydrogen and the inner sphere temperature transducers were calibrated by violently rocking the experiment in a shaker and recording the resistance of each transducer, which corresponds to the saturation temperature of hydrogen at atmospheric pressure. Each bridge was calibrated by using a decade box to obtain a voltage against resistance plot. Prior to each test, the pressure transducers were calibrated with standard pressure gages. Each of the calibration curves for the temperature and pressure transducers and for the bridges was curve fitted using a digital computer. The magnetic data tape from each test could then be fed into the digital computer along with the calibration curve fits, and an automatic data reduction program returned printed temperature and pressure data at half second intervals for every transducer.

For each of the tests, the experiment was prepared in an identical manner; only the actual test conditions were varied. The space between the inner and outer spheres was evacuated first with a mechanical pump and then with a diffusion pump. The experiment was cooled by circulating liquid nitrogen through the coils on the outer sphere. Then the inner sphere was filled with liquid hydrogen. The liquid-nitrogen cooling and the addition of the liquid hydrogen reduced the pressure in the space between the inner and outer spheres due to cryogenic pumping. A gas meter installed in the vent line together with the carbon resistors, described in the instrumentation section of this report, made it possible to determine the liquid level at the beginning of the test. The resistors accurately determine the liquid position at some time prior to the beginning of the test. The gas meter records the volume of vapor which then leaves the inner sphere. Measurements of the vapor temperature, at the gas meter, and the atmospheric pressure determine the density of the vapor. From a knowledge of the volume and density of the vapor, it is possible to calculate the mass of hydrogen which leaves the hydrogen container before the test begins.

The heater controller was set to maintain the desired heater temperature prior to the start of the test to eliminate transients. All the temperature instrumentation was checked for continuity with a digital ohmmeter and the recording system was turned on. At -1 minute the system began recording the data on magnetic tape. At zero time the vent valve was closed, and the experiment was allowed to self-pressurize to a nominal pressure of 100 psia (68.95 N/sq cm abs). The vent valve was then opened and the pressure was allowed to decay slowly. If a sufficient amount of liquid hydrogen still remained in the experiment, a similar test at a lower filling was run as soon as the new liquid level had been determined.

For the 21 quiescent tests, the experiment was supported directly from the ground.

This permitted the experiment to remain totally undisturbed throughout the test. For the homogeneous tests, the experiment was rocket violently in a shaker so that the contents of the inner sphere stayed thoroughly mixed.

EXPERIMENTAL RESULTS

The 21 quiescent tests consisted of eight tests with uniform heating, six tests with bottom heating, and seven tests with top heating. One of the homogeneous tests was uniformly heated and the other heated from the top. Initial percent fillings of 35, 50, and 80 percent were desired. The high fillings proved to be the most difficult to achieve since the boil-off was too great during the period of time required to check the experiment prior to a test. Heater temperatures of approximately 360°, 500°, and 575° R (200°, 278°, and 319° K) were used for the uniform heating tests, 500° and 575° R (278° and 319° K) for the bottom heating tests, and 425°, 500°, and 575° R (236°, 278°, and 319° K) for the top heating tests.

Figures 5 to 11, showing pressure and temperature as a function of time, present the data obtained from seven of the quiescent test runs. Only enough data symbols are included to identify the curves. Each of the figures is made up of four plots: (a) total pressure as a function of time, (b) outer-sphere and heater temperature as a function of time, (c) upper inner-sphere temperature as a function of time, and (d) lower inner-sphere temperature as a function of time. These seven tests were chosen as being representative of the 21 quiescent tests. Figures 5, 6, and 7 show the effects of three different percent fillings (34.9, 48.9, and 76.5 percent) for the uniformly heated and nearly constant heat-flux situation, approximately 65 Btu per hour per square foot (205 W/sq m). Figures 9, 10, and 11 show the effects of three different average heat fluxes, 17.1, 27.6, and 38.2 Btu per hour per square foot (54, 87, and 120 W/sq m), for an approximately half-full sphere which was heated only from the top. Figures 6, 8, and 10 show the effect of three different heating configurations, uniform bottom and top, for an approximately half-full sphere. The bottom heating test (fig. 8) had the same heat-transfer rate from the bottom heater as the bottom heater of the uniform heating test (fig. 6). The top heating test (fig. 10) had the same heat-transfer rate from the top heater as the top heater of the uniform heating test (fig. 6).

DISCUSSION OF EXPERIMENTAL RESULTS

Heat Transfer

Energy input to hydrogen container. - A first look at the data would tend to suggest to the reader that the plot of pressure as a function of time would be the most important

relation to consider when examining a group of tests which had identical heater temperatures. However, because the hydrogen vapor does become superheated and the top of the inner sphere does increase in temperature as a test proceeds, this approach can be quite misleading. The heating of the inner sphere causes a reduction in the heat transfer to the hydrogen due both to the reduction in radiant exchange and the energy which is required to increase the temperature of the container wall. Higher heater temperatures and lower percent liquid fillings cause increasing inner-sphere temperatures so that the average heat flux to the hydrogen is not a function only of heater temperature. As a result a better procedure is to compare the amount of heat that must be added to the hydrogen container to cause a given pressure rise for a particular set of conditions.

Temperature profiles. - For all the tests it was assumed that the temperature profiles were symmetric with respect to the vertical axis. In other words, at any time during a test all vertical planes passing through the center of the inner sphere would exhibit identical temperature patterns and the left side of such a plane would be a mirror image of the right side. This assumption is based on the fact that the inner sphere, heaters, vent tube, plastic support ring, instrumentation wires, and liquid-vapor interface all have symmetry with respect to the vertical axis and consequently there is no reason to anticipate that the temperature profiles would be different on opposite sides of the container. Based upon this assumption the amount of energy reradiated by the inner sphere can be calculated. The method of calculating the net radiant heat transfer and the conduction heat transfer is given in appendix C. Heat is added to the inner sphere by radiation from the heaters, by solid conduction through the vent tube, the plastic support ring, and the temperature transducer wires, and by gaseous conduction. Figure 12 is a plot of the rate of heat input as a function of time for each of the heat sources for a typical quiescent test. The gaseous conduction of heat was negligible for all the tests. The increasing temperature of the inner sphere accounts for the reduction in the radiant heat exchange from the upper heater, as time increases, due to the increasing reradiation from the inner sphere. The increasing temperature of the inner sphere also accounts for the decreasing and eventually negative conduction heat transfer from the vent tube since the inner sphere becomes hotter than the liquid-nitrogen cooled outer sphere, and heat is conducted away from the top of the inner sphere.

Summary of results. - Table I is a summary of the experimental results and the heat-transfer analysis. The initial percent filling was determined as explained in the PROCEDURE section. The pressure-rise rate is an average value obtained by dividing the difference between the pressure at the end of the test and atmospheric pressure in psia by the total test time. The bulk temperature was assumed to be the lowest recorded temperature, usually from temperature transducers 11 or 12. Dividing the change in the bulk temperature, during the test, by the change in the saturation temperature during the test, gives an indication of how much energy went into heating the liquid and, thus, how

nearly homogeneous the liquid is at the end of the test. The maximum change in the vapor temperature gives an indication of how much energy went into superheating the vapor. The average heat flux is determined by dividing the total energy input to the hydrogen as determined in appendix C by the test time and the surface area of the inner sphere. This average is then broken down into the heat flux through the liquid wetted walls and through the walls exposed to vapor. Breaking the heat flux up into parts in this manner clearly shows the effect of the increasing upper inner-sphere temperature which reduces the net radiant heat exchange.

Error Analysis

The two homogeneous tests were run for the purpose of checking the validity of the heat-transfer analysis and to get an estimate of the accuracy of the instrumentation. Figure 13 is a plot of sphere pressure as a function of heat added for the two homogeneous tests. One test was run with only the top heater installed, the other with both heaters installed. For both tests the experiment was shaken vigorously so that the hydrogen liquid and vapor were thoroughly mixed and at the saturation temperature corresponding to the absolute inner sphere pressure. Since the initial filling and pressure were known, a theoretical plot of homogeneous pressure against heat added (curves in fig. 13) was generated using the analytical technique presented in appendix B. Every 30 seconds the test data was used to perform a heat-transfer analysis (appendix C) and the heat added up to that point in time was plotted against the experimentally recorded pressure. These calculated points are identified by the symbols on figure 13. Comparing the data obtained from the heat-transfer analysis with the theoretical homogeneous line shows the combined experimental and analytical error. Ideally, the calculated points should fall on the theoretical line, but a maximum error of 2 psi (13.8 N/sq cm) or 2 percent of full scale was observed.

The homogeneous tests also provided a check on the accuracy of the inner-sphere temperature transducers since saturation temperature should be recorded during the entire test. In the previous discussion, it was impossible to separate the error associated with the pressure transducer from the error in the heat-transfer analysis. Here, it will be impossible to separate the error associated with the pressure transducer from the error associated with the temperature transducers. If it is first assumed that the pressure transducer is correct, the carbon-resistor temperature transducers indicate saturated conditions within a maximum of $\pm 0.6^{\circ}$ R ($\pm 0.3^{\circ}$ K) with an average error of -0.3° R (-0.2° K) in the range from 36° to 54° R (20° to 28° K). The platinum-surface temperature transducers indicate saturated conditions within a maximum of $+2.2^{\circ}$ R ($+1.2^{\circ}$ K) with an average error of $+0.9^{\circ}$ R ($+0.5^{\circ}$ K). Figure 14 is a plot of resistance

as a function of temperature for typical inner sphere temperature transducers. This figure shows that in the temperature range of 36° to 54° R (20° to 28° K) the carbon resistors undergo approximately a 70-ohm change in resistance while the platinum-surface transducer resistance changes only 4 ohms for each degree Rankine change in temperature. Consequently, at these low temperatures it would be expected that the carbon resistor temperature transducers would be more accurate. If it is now assumed that the carbon resistors are indicating the true saturation conditions, then the pressure transducer would have a maximum error of 2 psi (13.8 N/sq cm), or the same result obtained from the discussion associated with figure 13. Figure 14 is also useful in estimating the accuracy of the temperature transducers at higher temperatures. In the 200° to 300° R (111° to 167° K) range the carbon resistance transducers undergo approximately a 2-ohm change in resistance for each Rankine degree as compared with a 70-ohm change for each Rankine degree at the lower temperatures. This indicates that the resistors are less accurate by a factor of 35 at the higher temperatures so that errors as high as $\pm 20^{\circ}$ R ($\pm 11^{\circ}$ K) may be possible. Above 100° R (55° K) the platinum surface transducer resistance changed 7 ohms for each degree Rankine change in temperature so that these transducers should be slightly more accurate at higher temperatures than in the liquid-hydrogen temperature range. In summary, because both the heat-transfer analysis and the carbon-resistor temperature transducers indicated the same error in the pressure transducers, it is reasonable to assume that the pressure data is accurate within ± 2 psi (± 13.8 N/sq cm), that the platinum surface temperature transducers are accurate within $\pm 2^{\circ}$ R ($\pm 1.1^{\circ}$ K), and that the carbon-resistor temperature transducers are accurate to $\pm 0.3^{\circ}$ R ($\pm 0.2^{\circ}$ K) at low temperatures and $\pm 10^{\circ}$ R ($\pm 5.6^{\circ}$ K) at high temperatures.

Pressure-Rise Characteristics

Effect of heat-transfer rate and distribution. - Figure 15(a) shows the effect of heat-transfer rate and distribution on sphere pressure as a function of total heat added for the approximately 50 percent filled quiescent tests. The 50 percent filled tests were chosen because they represent the least complicated geometric situation where the liquid-vapor interface and the division between the upper and lower heaters are approximately in the same horizontal plane. It is readily apparent that the heating configuration is the primary factor affecting the slope of the pressure against heat added data. The heat-transfer rate had the least effect on the slope of the pressure as a function of heat added data for the bottom-heated tests with increasing influence on the uniformly heated and top-heated tests. However, the heat-transfer rate was definitely secondary in importance to the heating configuration.

Since the two coordinates, pressure and heat added, are the integrals over time of pressure-rise rate and heat-transfer rate, coincident test data indicate a linear relation between pressure-rise rate and heat-transfer rate; that is, doubling the heat-transfer rate will double the pressure-rise rate. For the bottom-heated tests this linear relation was followed almost exactly, but the uniformly heated tests, and to a greater degree, the top heating tests began to deviate. This indicates that the way in which energy was distributed in the liquid was unaffected by the rate of energy input, while the rate of energy input to the vapor greatly affected the resulting temperature or energy distribution.

Analysis based on the Rayleigh number indicates that the mode of heat transfer in the liquid would be turbulent convection (ref. 2). However, a summary of liquid-hydrogen boiling studies presented in reference 3 indicates that at the heat fluxes employed for these tests, nucleate boiling is quite likely to occur. An essentially uniform-temperature liquid bulk would be anticipated for either turbulent convection or boiling heat transfer. Because a uniform-temperature liquid bulk was experimentally observed, it is reasonable to assume that, at the lower heat fluxes, the heat-transfer mechanism in the liquid was dominated by turbulent convection with some boiling entering in at the higher heat fluxes. The heat-transfer processes which take place in the vapor are not clearly understood, but additional discussion will be presented after the energy-distribution analysis (appendix D) is introduced.

The theoretical surface evaporation and homogeneous lines which appear on figure 15(a) also help the reader to understand how the energy distribution within the hydrogen container affects the experimental results. Recall that the surface evaporation model is based on the concept of no-heating of the liquid bulk coupled with a saturated vapor while the homogeneous model has both saturated liquid and saturated vapor at all times. The top heating tests approach the surface evaporation model in one respect: the liquid is heated a very slight amount, but superheating of the vapor pushes the experimental data above the theoretical surface evaporation line. The bottom heating tests approach the homogeneous model in one respect: although the liquid is nearly saturated, some heating of the vapor causes superheating and the experimental data lie above the theoretical homogeneous line. The uniformly heated tests combine some heating of the liquid with superheating of the gas with the resulting data lying between the two extremes of top and bottom heating.

Effect of percent filling. - Figure 15(b) shows the effect of percent filling on the sphere pressure as a function of heat added for three uniformly heated tests. The data presented is for tests 3, 4, and 5. These three tests were chosen to demonstrate the effect of percent filling because the average heat flux for the three tests was nearly the same. Because of the increase in temperature of the upper part of the sphere, the low filling test had the lowest average heat flux. Based on the information obtained from figure 15(a) it would be expected that, if the average heat flux had been the same, the ex-

perimental data would have been somewhat closer together than that shown in figure 15(b). The obvious conclusion to be drawn from figure 15(b) is that the pressure-rise rate was only slightly affected by varying the percent filling, with a trend toward higher pressure-rise rates at higher fillings for the uniformly heated tests.

In order to understand why the pressure-rise rate is only slightly affected by the percent filling, reference is made to table I for the uniformly heated tests. The data for tests 3, 4, and 5 indicate that as the percent filling is increased, the liquid becomes less subcooled and the vapor becomes less superheated. These two effects tend to counterbalance each other. In contrast, the bottom heating tests exhibit decreasing pressure-rise rates with increasing filling, a result of the increased, nearly saturated liquid mass which is available to absorb the incoming energy. The top heating tests exhibit increasing pressure-rise rate with increasing filling. The increasing pressure-rise rate is a result of the increasing unheated liquid mass and the decreasing vapor volume which must absorb the incoming energy. Evidently, the uniformly heated tests are slightly dominated by the heating of the vapor which causes a small increase in the pressure rise rate with increasing filling.

Energy Distribution

Energy input to liquid and gaseous hydrogen. - To explain further the experimental results, an analysis was performed to determine what percentage of the incoming energy resulted in heating of the liquid bulk, the liquid thermal layer, evaporation of liquid, and superheating of the vapor. The details of these energy-distribution calculations will be found in appendix D. Figure 16 shows the inner-sphere temperature as a function of position for a typical quiescent test. The liquid-vapor interface is located at a height to radius ratio of 0.8. This figure shows that the temperature of the vapor space was only a function of the vertical coordinate, since the data for all the instrumentation, both centrally located and near the container wall, had the same temperature profile. Consequently, the energy distribution analysis was based on the assumption that the vapor space could be divided into horizontal uniform temperature disks. These disks, or elemental volumes, were then used to perform a summation (approximating an integration) to determine the total mass and internal energy of the vapor space at any time during the test. The total vapor internal energy is divided by the mass of vapor to determine the average vapor specific internal energy which together with the pressure defines an average vapor temperature. Knowledge of the change in internal energy and mass of the vapor as a function of time allows the calculation of the percentage of the energy input which superheated the vapor and caused evaporation. The percentage of the energy input which heated the liquid is determined by subtracting the input to the vapor and for evaporation from the total energy input calculated from the heat-transfer analysis. The mass

of the system is a constant so the mass of the liquid can be determined at any time by subtracting the mass of the vapor from the total initial mass. The average liquid internal energy is calculated from the initial conditions and the energy input to the liquid. Any average property of the liquid can now be determined since the pressure and average internal energy are known at any time. The average liquid density is calculated, which, together with the mass of the liquid, makes it possible to determine the percent filling at any time. The average percent filling is converted to an average liquid wetted area and multiplied by the wetted area heat-transfer rate to determine the energy input to the liquid wetted walls. The energy input to the liquid was further broken down into two parts: the energy which went into the bulk of the liquid and the energy which went into heating the thermal layer between the saturated liquid-vapor interface and the bulk of the liquid.

Figure 17 is a plot of inner-sphere temperature as a function of position for three heating configurations. Of particular interest are the temperature profiles in the liquid for the three tests (4, 10, and 19). It can be seen that the bulk temperature, or lowest recorded temperature, is representative of a large portion of the liquid mass. For the purposes of mathematical computation a linear temperature gradient from the bulk temperature to the saturation temperature at the interface was assumed. It is realized that, for some of the tests, this is a poor approximation to the actual temperature gradient, but the analysis based on this approximation helps to explain further how energy is transported and distributed within the liquid hydrogen.

Table II is a summary of the results of the energy distribution analysis. It will be noted that four tests were not included in the energy distribution analysis. Geometric considerations were responsible for the exclusion of these tests. The two low-percent-filling bottom heated tests had some direct heating of the vapor. The two high-percent-filling top heated tests had some direct heating of the liquid. It is impossible to separate the total energy input into the quantity which heated liquid and that which heated vapor in these configurations so the tests were not included.

Effect of heating configuration. - The bottom heating test results proved to be the easiest to understand and the least interesting. The energy input to the liquid wetted walls accounted for the heating of the bulk liquid, which was nearly saturated, the energy input to a thin liquid thermal layer, and the energy which went into evaporation (see table II). What heating of the vapor that did occur was a result of the small energy input to the dry walls. Considering the accuracy of the instrumentation and the analysis, it is quite possible that no thermal layer existed.

The top heating test results proved to be just the opposite: the hardest to understand and the most interesting. As before, the energy input to the liquid wetted walls approximately accounted for the heating of the liquid bulk, but the energy input to the dry walls heated the vapor, supplied the energy for evaporation, and heated the liquid thermal layer with over 50 percent of the total energy input ending up in the liquid thermal layer

(see table II). It seems reasonable to assume that the energy transfer from the vapor to the liquid was intermolecular in nature. The fact that the lines of constant temperature in the vapor were horizontal, with increasing temperature at higher vertical positions, may rule out the possibility of any convective flow. It is possible that an involved conduction analysis could predict both the vapor and the liquid thermal layer gradients; however, a detailed analysis was not undertaken. An order-of-magnitude analysis using the observed temperature gradients and heat-transfer rates has indicated that conduction could be the primary mode of energy exchange. It was not felt that the experiment design or the accuracy of the instrumentation and analysis lent itself to further pursuit of this line of thought.

The results of the analysis on the uniformly heated tests were easily identified as being the combined results of the top heating and bottom heating tests. The energy input to the dry walls heated the vapor, supplied the necessary energy for evaporation, and heated most of the liquid thermal layer. The energy input to the liquid wetted walls heated the liquid bulk and a portion of the liquid thermal layer (see table II). It is quite possible that the inaccuracies in the analysis would account for the portion of the heating of the liquid thermal layer which came from the liquid wetted walls. These inaccuracies come from (1) the assumption of a linear temperature gradient in the liquid thermal layer, (2) the fact that the energy passing through the liquid wetted walls near the interface must add to the thermal layer, and (3) the consideration of the fact that, as the test proceeds, the liquid thermal layer grows and liquid which was previously included in the bulk now becomes part of the thermal layer. The pressure-rise rate in the hydrogen container for the uniformly heated tests is primarily a function of the energy input to the vapor since the input to the liquid wetted walls primarily heats the liquid bulk. The only contribution which heating the liquid makes to the container pressure is due to the thermal expansion of the liquid. Liquid hydrogen does have a relatively high coefficient of thermal expansion, but this effect is secondary to the energy input to the vapor for determining the rate of pressure rise.

Entropy Analysis

To summarize the experimental results obtained from the 21 quiescent tests, a simple calculation was performed. The average liquid and vapor temperatures, obtained from the energy distribution analysis, together with the pressure at the beginning and end of each test were used to compute the average liquid and vapor specific entropy. Knowledge of the mass of the liquid and vapor both at the start and end of the test made it possible to determine the total change in system entropy during the test. This change in system entropy was divided by the change in entropy of the corresponding homogeneous model and the resulting dimensionless parameter was termed the homogeneity factor.

Figure 18 is a plot of the homogeneity factor as a function of the average heat-transfer rate for the quiescent tests.

The thermodynamic property entropy is often associated with probability. It was with this thought in mind that the change in entropy of a real system, as compared with a theoretical homogeneous model, was chosen as the single parameter most suitable for summarizing the experimental results. A homogeneity factor equal to unity would be for a homogeneous system. In contrast, systems with low homogeneity factors exhibit large temperature gradients. If isolated, these systems would decay to the more probable uniform temperature situation found in a homogeneous system. The length of the lines on figure 18 is indicative of the range of heat flux that was explored for each percent filling and heating configuration while the thickness of the lines represents the author's confidence limits. Nothing new or unexpected resulted from this entropy calculation. Once again, it is apparent that the heating configuration is the most important variable affecting the final state of the system. The heat-transfer rate was of significant influence only on the top heating tests. For the bottom heating tests, the high percent fillings were more nearly homogeneous because the vapor mass, which was slightly superheated, was smaller. For the top heating tests the high fillings were less homogeneous because the mass of the liquid bulk, which essentially did not change temperature, was larger. The uniformly heated tests showed the influence of both the top- and bottom-heating effects with the top heating dominating the overall final system conditions.

SUMMARY OF RESULTS

A nonventing 9-inch- (23 cm) diameter spherical tank partially filled with liquid hydrogen, was subjected to 21 quiescent self-pressurization tests. The tests were begun at 1 atmosphere pressure and terminated at a maximum pressure of nominally 100 psia (68.95 N/sq cm abs). The hydrogen tank was subjected to various combinations of the variables; percent filling, heat transfer rate, and either top heating, bottom heating, or uniform heating. The following results were obtained:

1. The rate of pressure rise was affected most by heater configuration, being greatest for the tests where the vapor was heated directly, least for the tests where the liquid was heated directly.

2. The pressure-rise rate increased almost linearly with increasing heat-transfer rate.

3. For the uniformly heated tests the pressure-rise rate was only slightly affected by varying the percent filling.

4. Appreciable energy transfer from the vapor to the liquid causing evaporation and liquid heating occurred during both the uniform heating and top heating tests.

5. Nearly saturated liquid temperatures were recorded throughout the liquid for the bottom heating tests.

6. Two homogeneous tests validated the heat-transfer analysis and indicated the error associated with both the pressure and temperature transducers.

Lewis Research Center,
National Aeronautics and Space Administration,
Cleveland, Ohio, March 30, 1967,
124-09-03-01-22.

APPENDIX A

SYMBOLS

A	surface area, sq ft; sq m
B_{jl}	absorption factor
C_p	specific heat, Btu/(lb)(^oR); J/(kg)(^oK)
F	angle factor
k	thermal conductivity, Btu/(hr)(ft)(^oR); W/(m)(^oK)
L	length, ft; m
m	mass, lb; kg
P	pressure, lb/sq in. abs; N/sq cm
pf	filling by volume, percent
Q	heat added, Btu; J
q	heat transfer rate, Btu/hr; W
r	reflectivity
T	absolute temperature, ^oR; ^oK
t	time, hr
U	total internal energy, Btu; J
u	specific internal energy, Btu/lb; J/kg
V	volume, cu ft; cu m
x	linear distance, ft; m
ϵ	emissivity
ρ	density, lb/cu ft; kg/cu m
σ	Stefan-Boltzmann constant, 0.1713×10^{-8} Btu/(hr)(sq ft)($^oR^4$); 5.6697×10^{-8} W/(sq m)($^oK^4$)

Subscripts:

a	absorbed
av	average
b	liquid bulk
ev	evaporation
f	final or any intermediate state
gc	gaseous conduction
i	initial state
j	summation variable
L	at x = L
ℓ	liquid
l	liquid thermal layer
m	mean or average value
max	maximum
n	summation variable
r	radiant
rr	reradiated
s	system
sat	saturation
sc	solid conduction
st	stored
v	vapor
w	wall
0	at x = 0
1	inner sphere
2	upper heater
3	lower heater
4	outer sphere

APPENDIX B

THERMODYNAMIC ANALYSIS

One method of analyzing a system thermodynamically is to define the conditions at the beginning and the end of a process; then the necessary input to the system can be determined. For the problem of a liquid-hydrogen storage tank, which is sealed at the beginning of the test, the initial condition is that the tank contains a homogeneous mixture at atmospheric pressure with a known percent filling by volume. The final condition is defined by the model being considered. For a nonexpanding closed system, the input is heat, and, as stated by the first law of thermodynamics

$$Q = \Delta U \tag{B1}$$

Equation (B1) may be written in the form

$$Q = U_f - U_i = (m_{\ell,f}u_{\ell,f} + m_{v,f}u_{v,f}) - (m_{\ell,i}u_{\ell,i} + m_{v,i}u_{v,i}) \tag{B2}$$

The density and specific internal energy of each phase at state i can be found if the system is known to be homogeneous and at the saturation temperature corresponding to atmospheric pressure (ref. 4). The total internal energy at state i can then be determined because

$$m_{\ell,i} = \rho_{\ell,i}\frac{(pf)_i}{100}V \tag{B3}$$

$$m_{v,i} = \rho_{v,i}\left[1 - \frac{(pf)_i}{100}\right]V \tag{B4}$$

For a closed nonexpanding system, the mass of the liquid plus the mass of the vapor is a constant; consequently, the system density is a constant

$$\rho_s = \frac{(pf)_i}{100}\rho_{\ell,i} + \left[1 - \frac{(pf)_i}{100}\right]\rho_{v,i} \tag{B5}$$

For the homogeneous model, state f (and thus the density and internal energy of each phase) is defined by the fact that the system is homogeneous and is at the saturation temperature corresponding to the system pressure. Equation (B5), written for state f, can be solved for the percent filling at state f

$$(pf)_f = \frac{\rho_s - \rho_{v,f}}{\rho_{\ell,f} - \rho_{v,f}} (100) \tag{B6}$$

The total internal energy at state f can then be determined since

$$m_{\ell,f} = \rho_{\ell,f} \frac{(pf)_f}{100} V \tag{B7}$$

and

$$m_{v,f} = \rho_{v,f} \left[1 - \frac{(pf)_f}{100}\right] V \tag{B8}$$

The amount of heat required to reach state f for the homogeneous model can now be calculated by using equation (B2).

For the surface-evaporation model, state i is the same as that for the previous model so that the total internal energy at state i is found by the identical procedure. The surface-evaporation model is based on the concept that all of the energy goes into evaporating the liquid and maintaining the vapor at the saturation temperature. If it is assumed that the liquid is incompressible, then the density and internal energy of the remaining liquid will be unaltered by the process; that is, $\rho_{\ell,i} = \rho_{\ell,f}$ and $u_{\ell,i} = u_{\ell,f}$. The density and internal energy of the vapor are defined by the fact that the vapor is homogeneous and at the saturation temperature corresponding to the final system pressure. Equation (B5), written for state f, can be solved for the percent filling at state f:

$$(pf)_f = \frac{\rho_s - \rho_{v,f}}{\rho_{\ell,i} - \rho_{v,f}} 100 \tag{B9}$$

The mass of liquid and vapor at state f can then be determined since

$$m_{\ell,f} = \rho_{\ell,i} \frac{(pf)_f}{100} V \tag{B10}$$

and

$$m_{v,f} = \rho_{v,f} \left[1 - \frac{(pf)_f}{100}\right] V \tag{B11}$$

The total internal energy at state f can now be determined, and from equation (B2) the heat required to reach state f for the surface-evaporation model can be calculated.

APPENDIX C

HEAT-TRANSFER ANALYSIS

The amount of energy absorbed by the contained hydrogen is equal to the heat transferred to the sphere by radiation, solid conduction, and gaseous conduction minus the amount of energy stored in the container itself; that is,

$$Q_a = (q_r + q_{sc} + q_{gc})\Delta t - Q_s \tag{C1}$$

The amount of heat transferred by thermal radiation from the heated intermediate sphere to the inner sphere is determined by the method presented in reference 2. For the radiant exchange calculations the outside of the inner sphere is assigned the number 1, the inside of the upper heater number 2, the inside of the lower heater number 3, and the inside of the outer sphere number 4. The effect of the small openings in the heaters for tubing, wires, and supports was neglected. The net rate of radiant heat absorbed by the inner sphere when both heaters are installed is

$$q_1 = \sum_{j=1}^{3} \sigma B_{j1} \epsilon_j A_j T_j^4 - \sigma \epsilon_1 A_1 T_1^4 \tag{C2}$$

where B_{j1}, the absorption factor, is defined as the fraction of the total radiant-energy emission of surface j which is absorbed by surface 1. The absorption factors are determined by solution of the following simultaneous equations:

$$(F_{11}r_1 - 1)B_{11} + F_{12}r_2B_{21} + F_{13}r_3B_{31} + F_{11}\epsilon_1 = 0 \tag{C3}$$

$$F_{21}r_1B_{11} + (F_{22}r_2 - 1)B_{21} + F_{23}r_3B_{31} + F_{21}\epsilon_1 = 0 \tag{C4}$$

$$F_{31}r_1B_{11} + F_{32}r_2B_{21} + (F_{33}r_3 - 1)B_{31} + F_{31}\epsilon_1 = 0 \tag{C5}$$

This technique treats all diffuse-radiation circumstances and requires only a knowledge of the geometry of the three surfaces, the average temperature of the surfaces, and the emissivity of the surfaces. Lewis Research Center personnel experimentally obtained the emissivity (fig. 19) using a sample surface identical to the inner surface of the heaters and the outer surface of the hydrogen container.

When one of the hemispherical heaters was removed in order to obtain only top or

bottom heating, the outer-sphere surface 4, had to be substituted for the removed heater, surface 2 or 3, in equation (C2) and subsequent calculations. The inside of the outer sphere and the outside of the heaters were gold plated. The analysis was nearly insensitive to the value of emissivity for these surfaces so an approximate value of 0.10 was assumed. Because of the variation in temperature of the inner sphere, the last term in equation (C2) was expressed as an integral and called the inner-sphere reradiated heat flux

$$q_{1,rr} = \int_{A_1} \sigma \epsilon T^4 \, dA \tag{C6}$$

where A_1 is the surface area of the inner sphere. This integral was approximated by the summation

$$q_{1,rr} \approx \sum_{j=1}^{n} \sigma \epsilon_j T^4 \, \Delta A_j \tag{C7}$$

As explained in the DISCUSSION OF EXPERIMENTAL RESULTS section, the temperature of the inner sphere was only a function of the vertical coordinate so that horizontal uniform temperature sections could be used to divide the sphere into elemental surface areas. A digital computer was used to curve fit the emissivity as a function of temperature curve and the inner-sphere temperature as a function of position curves for each time interval. An average temperature for each elemental area was used to determine the local emissivity, and the summation was performed every 30 seconds by using a digital computer.

The energy stored in the container at any time interval was also expressed as an integral

$$Q_{st} = \int_{V_{1,w}} C_p \rho T \, dV \tag{C8}$$

where $V_{1,w}$ is the volume of the container wall. This integral was approximated by the summation

$$Q_{st} \approx \sum_{j=1}^{n} \rho C_{p,j} T_j \, \Delta V_j \tag{C9}$$

Assuming the same temperature distribution, a digital computer was used to curve fit the stainless-steel specific heat as a function of temperature curve found in figure 20 (ref. 5) and the inner-sphere temperature as a function of position curves for each time interval. An average temperature for each elemental volume was used to determine the specific heat and the summation was performed every 30 seconds by using a digital computer.

The differential equation and boundary conditions for one-dimensional heat transfer by solid conduction are the following:

$$\frac{d}{dx}\left(k\frac{dT}{dx}\right) = 0 \begin{cases} \text{at } x = 0, & T = T_0 \\ \text{at } x = L, & T = T_L \end{cases} \tag{C10}$$

At the very low temperatures encountered with the use of liquid hydrogen, the thermal conductivity of most materials is highly temperature dependent and can be expressed as some function of the absolute temperature. Substituting the boundary conditions in equation (C10) and integrating (ref. 2) result in

$$\frac{q}{A} = k_m \frac{T_0 - T_L}{L} \tag{C11}$$

where

$$k_m = \frac{1}{T_L - T_0} \int_{T_0}^{T_L} k(T)dT \tag{C12}$$

Figure 21 shows the stainless-steel thermal conductivity as a function of temperature (ref. 5) and the curve fit which was used to perform the necessary integration in equation (C12). Figure 22 shows the plastic support ring thermal conductivity as a function of temperature and the curve fit which was used to perform the necessary integration in equation (C12). The data for this figure was obtained experimentally by Lewis Research Center personnel using a sample piece of polychlorotrifluoroethylene plastic identical to that used in the experiment.

For all the tests, the heat transfer due to gaseous conduction through the vacuum space, was negligible, since vacuum levels were always less than 10^{-4} micron of mercury.

APPENDIX D

ENERGY DISTRIBUTION ANALYSIS

The total volume of the hydrogen container as it appears in this analysis included the volume of the plumbing up to the seal-off point of the experiment. Expansion of the container due to the increasing pressure was neglected.

The total test time was divided into 30-second intervals, and the following calculations were performed for each time interval. As a first approximation, it was assumed that the liquid level did not change between successive time intervals so that the volume of vapor could be determined.

As explained in the DISCUSSION OF EXPERIMENTAL RESULTS section, the temperature of the hydrogen vapor was only a function of the vertical coordinate so that horizontal uniform temperature sections could be used to divide the vapor space into elemental volumes. Each elemental volume then approximated a region of constant temperature and pressure. Since two thermodynamic properties are known, for each elemental volume, any other property can be determined. The properties of particular interest are the density and specific internal energy. The equations which were used to generate the hydrogen tables (ref. 4) were curve fitted using a digital computer so that the desired properties were readily available once the pressure and temperature were known. This made it possible to determine the total internal energy and mass of the vapor at any time.

$$m_v = \int_{V_v} dm_v \tag{D1}$$

$$U_v = \int_{V_v} u_v \, dm_v \tag{D2}$$

These two integrals were approximated by the summations

$$m_v \approx \sum_{j=1}^{n} \rho_{v,j} \, \Delta V_{v,j} \tag{D3}$$

$$U_v \approx \sum_{j=1}^{n} u_{v,j} \rho_{v,j} \, \Delta V_{v,j} \tag{D4}$$

At any time these summations can be evaluated by using a digital computer. It is first

necessary to curve fit the vapor temperature against position data for the test times of interest. The computer can then determine the necessary properties, from the hydrogen property curve fits, for each elemental volume and perform the necessary mathematical operations. The energy input to the vapor during any time interval is

$$Q_v = U_{v,f} - U_{v,i}$$

The change in the mass of the vapor is

$$\Delta m_v = m_{v,f} - m_{v,i} \tag{D5}$$

The energy input that results in evaporation is

$$Q_{ev} = (\Delta m_v)(\text{heat of vaporization}) \tag{D6}$$

The energy input to the liquid is determined by subtracting the energy input to the vapor and the energy input that results in evaporation from the total energy input to the container.

$$Q_\ell = Q_1 - Q_v - Q_{ev} \tag{D7}$$

To explore further the energy distribution within the liquid phase, it was assumed that the liquid consisted of a uniform temperature region known as the bulk and a region of linear temperature change between the bulk and the liquid-vapor interface known as the thermal layer. This assumption is considered in detail in the DISCUSSION OF EXPERIMENTAL RESULTS section. The bulk temperature, at any time, is determined from the instrumentation and the thermal layer average temperature is

$$T_\ell = \frac{T_b + T_{sat}}{2} \tag{D8}$$

Since the liquid-vapor interface is always at the saturation temperature, the average internal energy of the liquid initially corresponds to the saturated temperature and pressure and at any later time is

$$u_{\ell,av} = u_{\ell,i} + \frac{Q_\ell}{m_\ell} \tag{D9}$$

where

$$m_\ell = m_{\ell,i} - \Delta m_v$$

At any time the energy stored in the liquid must be equal to the sum of the energy stored in the two regions.

$$m_\ell u_{\ell,av} = m_b u_b + m_l \frac{u_b + u_{sat}}{2} \tag{D10}$$

The total mass of liquid is equal to the sum of the mass of liquid in the two regions.

$$m_\ell = m_b + m_l \tag{D11}$$

Combination of equations (D10) and (D11) yields:

$$m_b = m_\ell \frac{(u_{\ell,sat} + u_b - 2u_{\ell,av})}{u_{\ell,sat} - u_b} \tag{D12}$$

All the liquid is initially saturated so the energy input to the bulk is

$$Q_b = m_{b,f} u_{b,f} - m_{\ell,i} u_{\ell,sat,i} \tag{D13}$$

Subtracting the energy input to the bulk from the total energy input to the liquid yields

$$Q_l = Q_\ell - Q_b \tag{D14}$$

The percent filling of the inner sphere at any time is

$$pf = \frac{m_\ell}{\rho_{\ell,av} V} \times 100 \tag{D15}$$

where $\rho_{\ell,av}$ is determined by using the computer and the values of the total sphere pressure and $u_{\ell,av}$ as input. This new value of percent filling allows the vapor volume to be recomputed and the calculations are performed again starting with equation (D1). This cycle is repeated until the liquid mass changes by less than 0.1 percent; the computer then proceeds to the next time interval.

REFERENCES

1. Clark, J. A.: A Review of Pressurization, Stratification, and Interfacial Phenomena. International Advances in Cryogenic Engineering. Vol. 10, K. D. Timmerhaus, ed., Plenum Press, 1965, pp. 259-283.

2. Gebhart, Benjamin: Heat Transfer. McGraw-Hill Book Co., Inc., 1961.

3. Drayer, D. E.; and Timmerhaus, K. D.: An Experimental Investigation of the Individual Boiling and Condensing Heat-Transfer Coefficients for Hydrogen. Advances in Cryogenic Engineering. Vol. 7, K. D. Timmerhaus, ed., Plenum Press, 1962, pp. 401-412.

4. Roder, Hans M.; and Goodwin, Robert D.: Extended Tables of Provisional Thermodynamic Functions for Para-Hydrogen (British Units); in Liquid, Fluid and Gaseous States at Pressures to 5000 PSI, 36 to 180^{o} R and at Pressures to 1500 PSIA, 140 to 540^{o} R. Rep. No. 7220, National Bureau of Standards, Jan. 3, 1962.

5. Scott, Russell B.: Cryogenic Engineering. D. Van Nostrand Co., Inc., 1959.

TABLE I. - SUMMARY OF EXPERIMENTAL RESULTS AND HEAT-TRANSFER ANALYSIS

Test number	Initial filling, percent	Pressure rise rate		Liquid temperature ratio, $\Delta T_b/\Delta T_{sat}$	Maximum vapor temperature change		Unit area heat-transfer rate q/A_1					
							Average		Wetted area		Dry area	
		psi/min	N/sq m		^oR	^oK	Btu/(hr)(sq ft)	W/sq m	Btu/(hr)(sq ft)	W/sq m	Btu/(hr)(sq ft)	W/sq m
Uniform heating												
1	34.6	3.5	402	0.55	110	61.1	17.5	55	20.0	63	15.7	49
2	51.4	3.6	414	.46	115	63.9	18.2	57	20.0	63	16.4	52
3	34.9	11.3	1298	.62	212	117.8	59.9	189	80.3	253	45.8	144
4	48.9	13.5	1551	.47	200	111.1	65.0	205	80.7	254	48.9	154
5	76.5	17.0	1953	.32	159	88.3	72.6	229	80.5	254	54.1	171
6	36.8	19.3	2218	.61	258	143.3	105.4	332	148.0	466	74.5	235
7	50.7	23.6	2712	.47	245	136.1	111.6	352	142.7	450	78.4	247
8	77.2	30.3	3481	.31	182	101.1	128.6	405	141.9	447	97.7	308
Bottom heating												
9	29.3	5.9	678	0.99	85	47.2	39.5	125	78.5	247	16.3	51
10	49.0	4.9	563	.99	109	60.5	44.6	141	81.7	258	5.1	16
11	73.5	3.6	414	.97	73	40.5	42.6	134	59.5	188	2.9	9
12	31.0	11.0	1264	.95	87	48.3	73.3	231	146.6	462	27.3	86
13	47.8	8.6	988	.96	90	50.0	75.2	237	144.9	457	3.0	9
14	74.0	6.3	724	.92	54	30.0	75.7	239	105.4	332	3.5	11
Top heating												
15	36.5	4.6	529	0.10	81	45.0	15.5	49	1.5	5	25.2	79
16	50.5	5.8	666	.07	85	47.2	17.1	54	2.2	7	32.2	101
17	80.4	8.8	1011	.05	99	55.0	19.6	62	13.8	43	34.0	107
18	34.3	8.2	942	.11	118	65.5	24.2	76	2.8	9	38.2	120
19	51.2	11.2	1287	.06	123	68.3	27.6	87	4.6	14	51.7	163
20	47.7	18.5	2126	.05	153	85.0	38.2	120	3.5	11	71.0	224
21	77.0	30.3	3481	.04	158	87.8	53.6	169	42.6	134	77.8	245

TABLE II. - RESULTS OF ENERGY-DISTRIBUTION ANALYSIS

Test number	Average filling, percent	Energy input to liquid wetted walls, percent of total	Heat added, percent of total energy input				
			Liquid	Vapor	Evaporation	Bulk liquid	Liquid thermal layer
Uniform heating							
1	35.8	46.4	77.4	8.8	13.8	32.5	44.9
2	52.9	57.2	83.0	6.7	10.3	51.7	31.3
3	36.7	54.9	76.1	18.1	5.8	39.1	37.0
4	50.4	62.7	79.4	15.4	5.2	58.4	21.0
5	78.2	77.5	91.1	7.7	1.2	64.6	26.5
6	38.4	59.2	74.4	22.0	3.6	47.8	26.6
7	52.2	66.0	77.4	18.7	3.9	65.5	11.9
8	78.7	77.1	90.7	8.7	.6	63.8	26.9
Bottom heating							
10	52.8	94.4	85.4	3.5	11.1	82.6	2.8
11	79.4	98.2	97.0	.9	2.1	95.6	1.4
13	50.9	98.1	84.6	3.6	11.8	80.9	3.7
14	79.9	98.8	96.8	.9	2.3	96.8	0
Top heating							
15	36.9	4.1	70.9	9.7	19.4	5.6	65.3
16	50.7	6.6	70.8	8.4	20.8	6.2	64.6
18	34.6	4.5	67.6	14.6	17.8	8.0	59.6
19	51.2	8.6	66.2	12.4	21.4	5.4	60.8
20	47.7	4.4	59.3	18.9	21.8	4.8	54.5

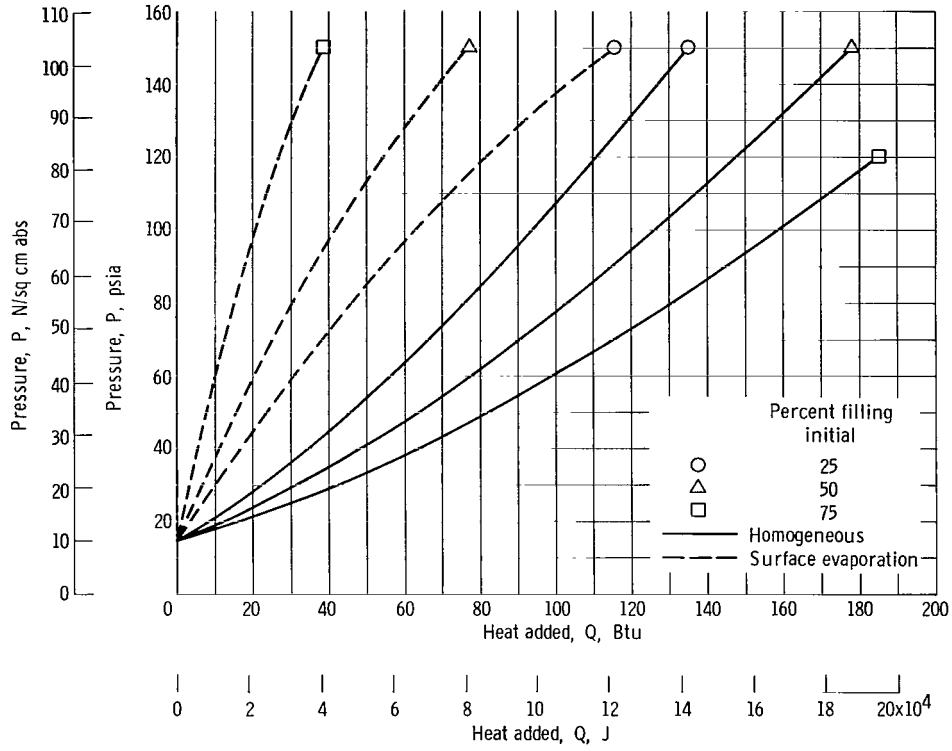

Figure 1. - Tank pressure as function of heat added for two-energy distribution models. Tank size, 1 cubic foot (2.832×10^{-2} cu m).

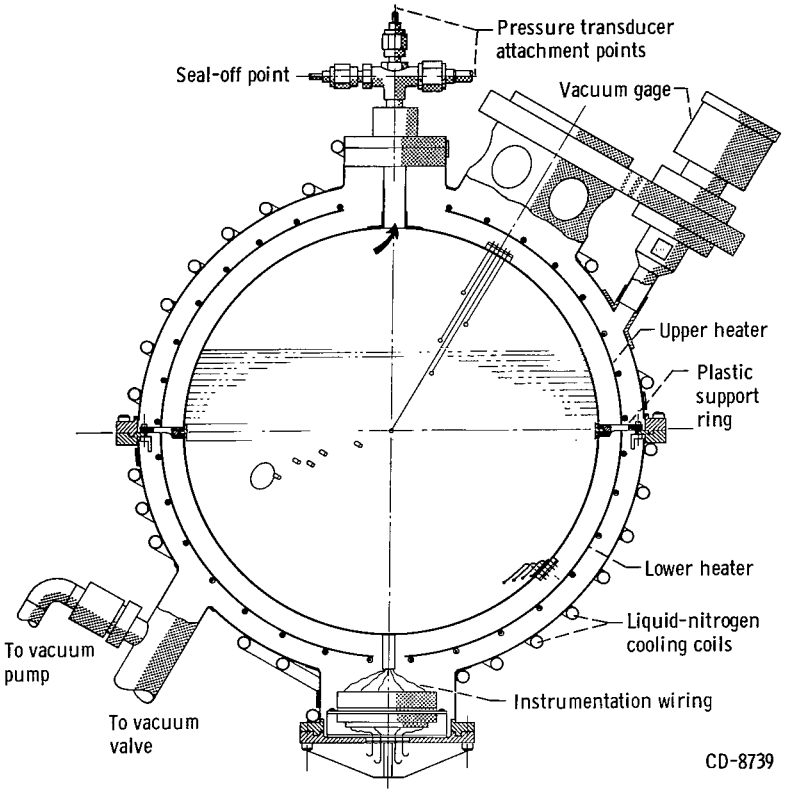

Figure 2. - Schematic drawing of liquid-hydrogen experiment.

Carbon resistor temperature transducer	Distance from wall,	
	in.	cm
R-1	4.50	11.43
R-6	3.30	8.30
R-2	2.90	7.37
R-3	2.20	5.59
R-7	2.11	5.36
R-4	1.86	4.72
R-8	1.66	4.22
R-9	1.18	3.00
R-5	1.02	2.59
R-11,17	.60	1.52
R-10	.50	1.27
R-12, 18	.40	1.02
R-15, 19	.20	0.51
R-20	.02	0.05

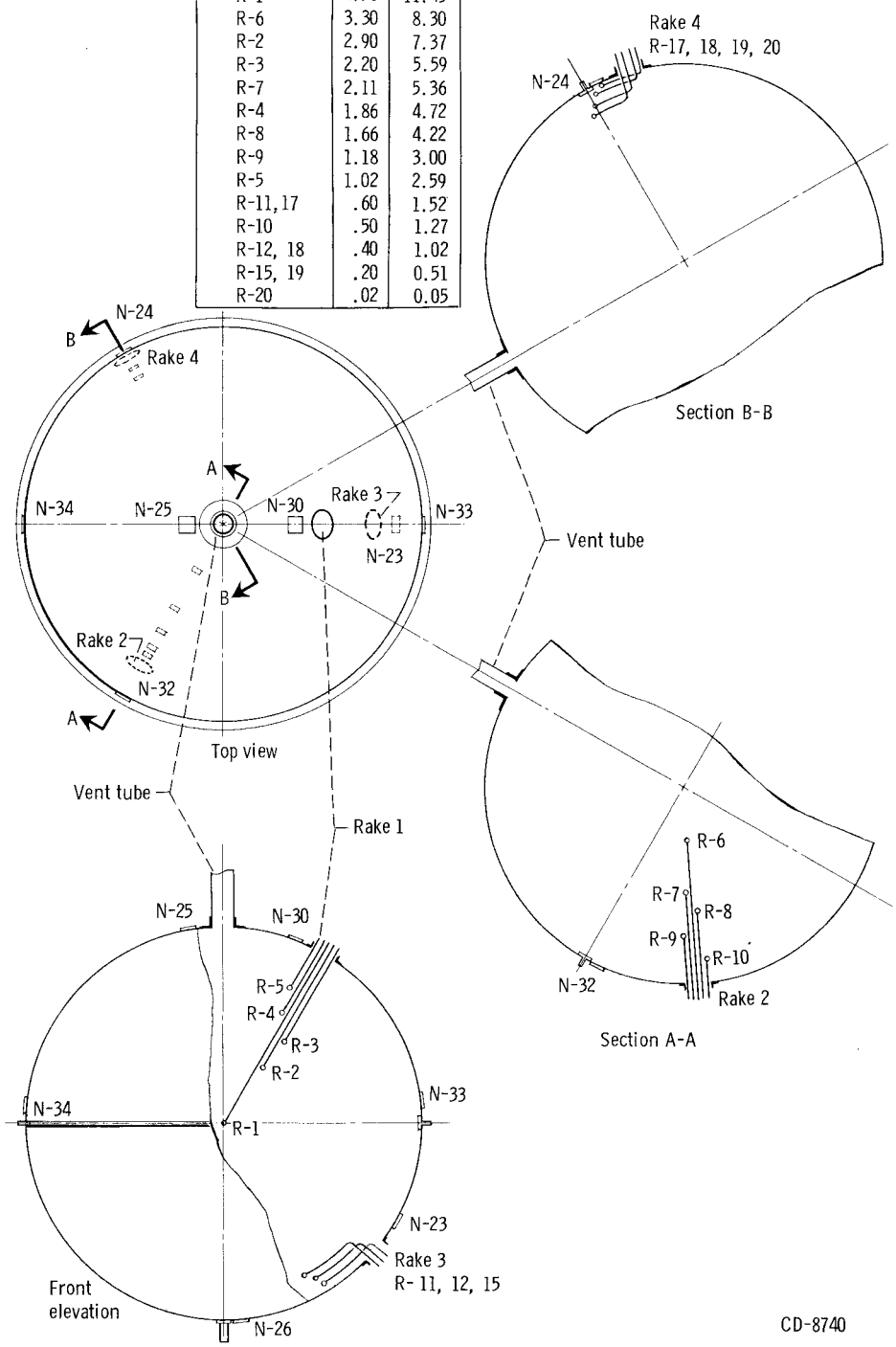

Figure 3. - Inner sphere temperature transducer locations. Numbers preceeded by N denote surface temperature transducers.

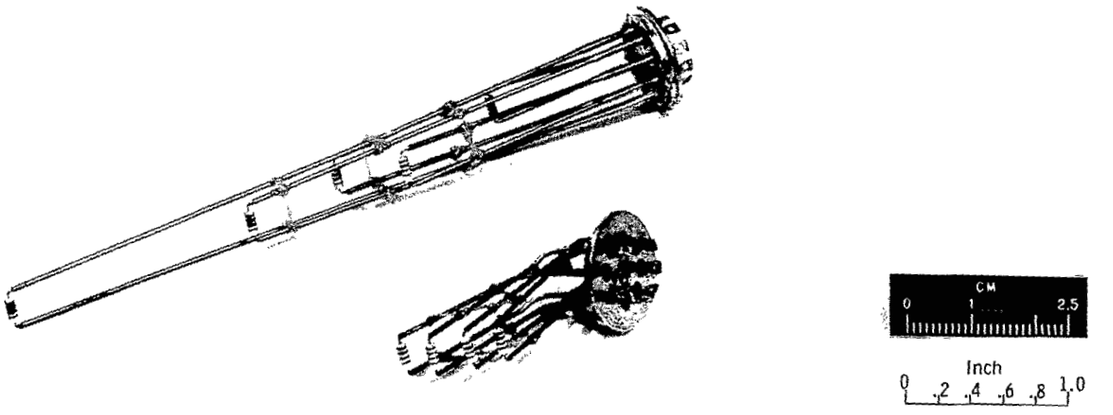

Figure 4. - Carbon resistor rakes.

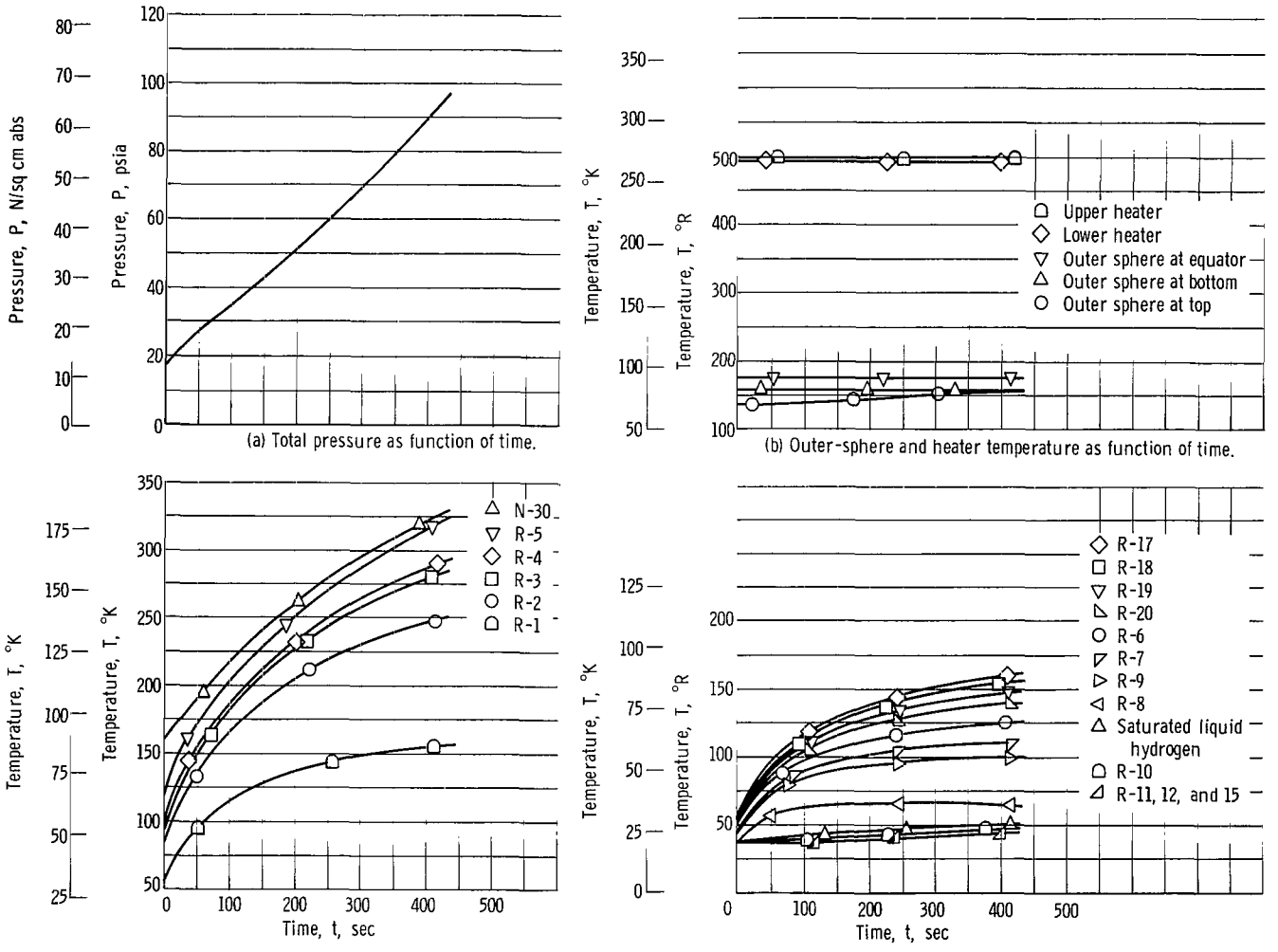

Figure 5. - Test 3. Uniform heating; initial filling, 34.9 percent; average heat flux, 59.9 Btu per hour per square foot (189 W/sq m). (See fig. 3 for location of transducers.)

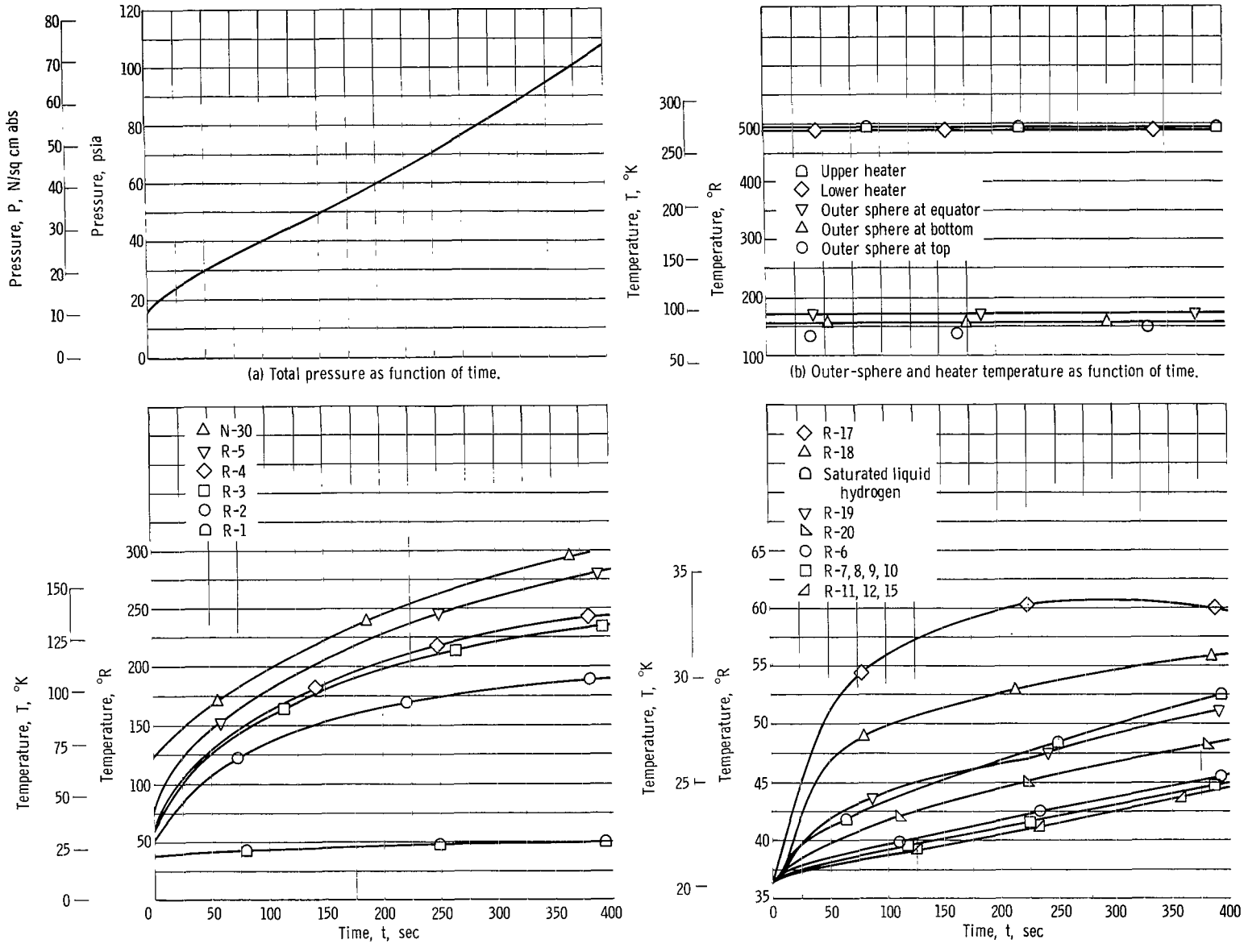

Figure 6. - Test 4. Uniform heating; initial filling, 48.9 percent; average heat flux, 65.0 Btu per hour per square foot. (204 W/sq m).

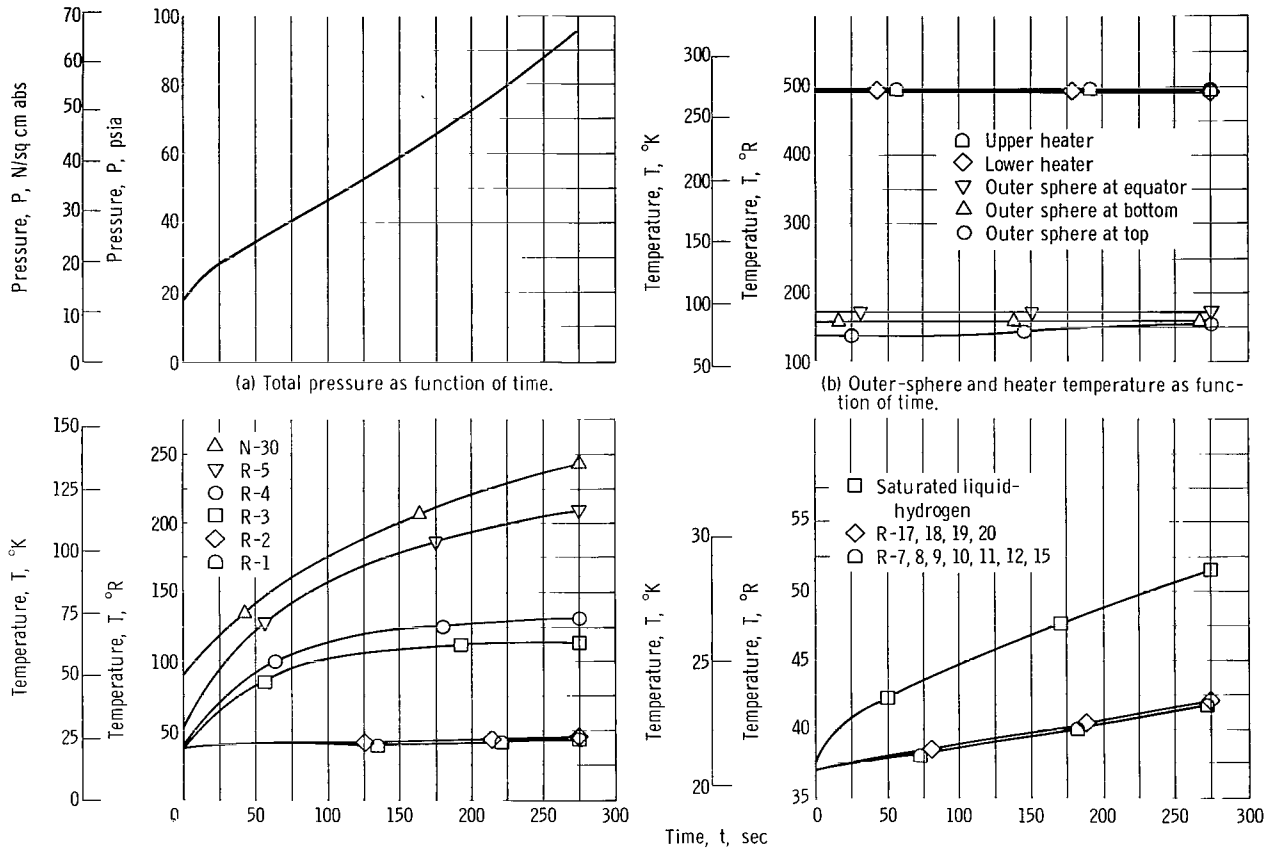

Figure 7. - Test 5. Uniform heating; initial filling, 76.5 percent; average heat flux, 72.6 Btu per hour per square foot (229 W/sq m). (See fig. 3 for location of transducers.)

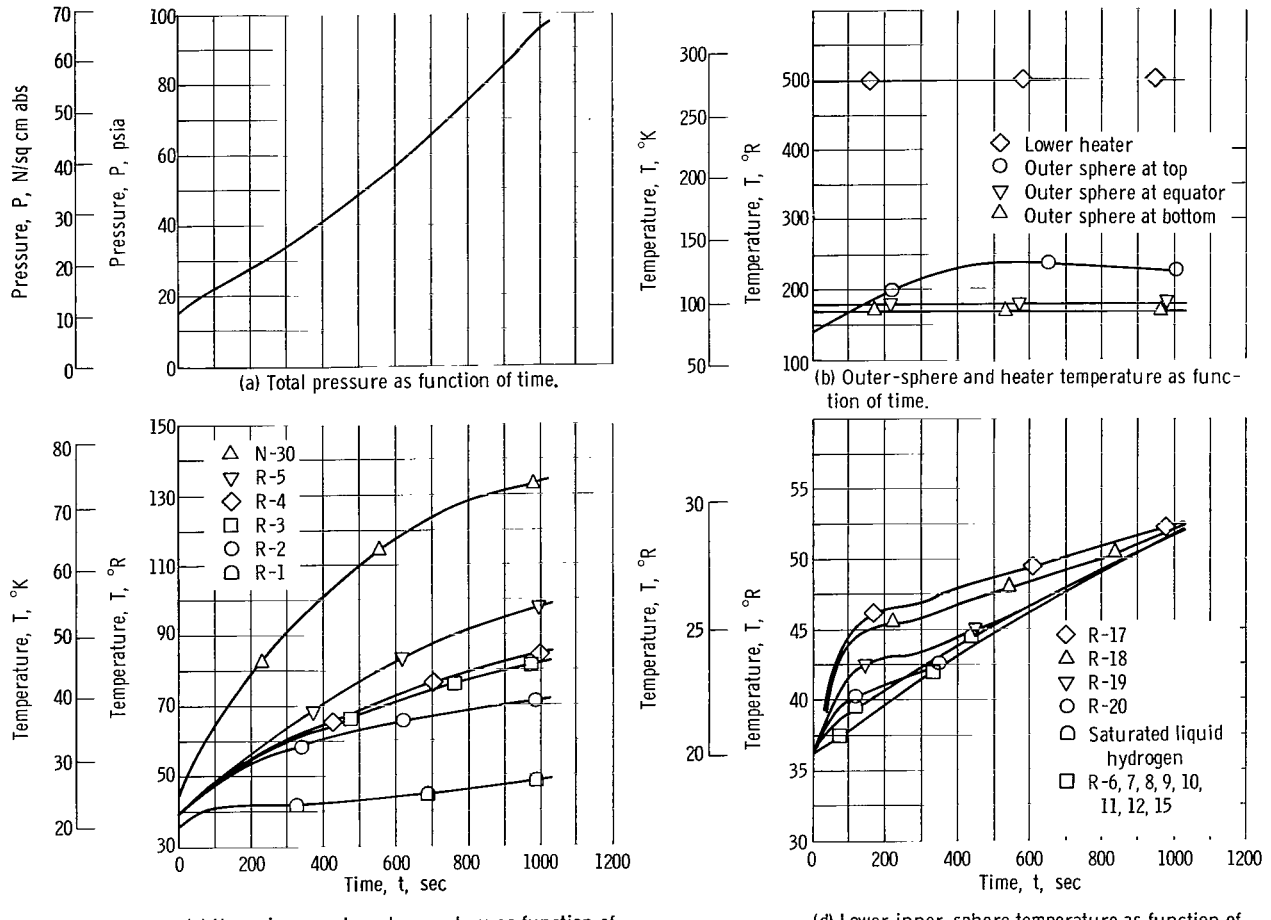

(a) Total pressure as function of time.

(b) Outer-sphere and heater temperature as function of time.

(c) Upper inner-sphere temperature as function of time.

(d) Lower inner-sphere temperature as function of time.

Figure 8. - Test 10. Bottom heating; initial filling, 49 percent, average heat flux, 44.6 Btu per hour per square foot (140 W/sq m). (See fig. 3 for location of transducers.)

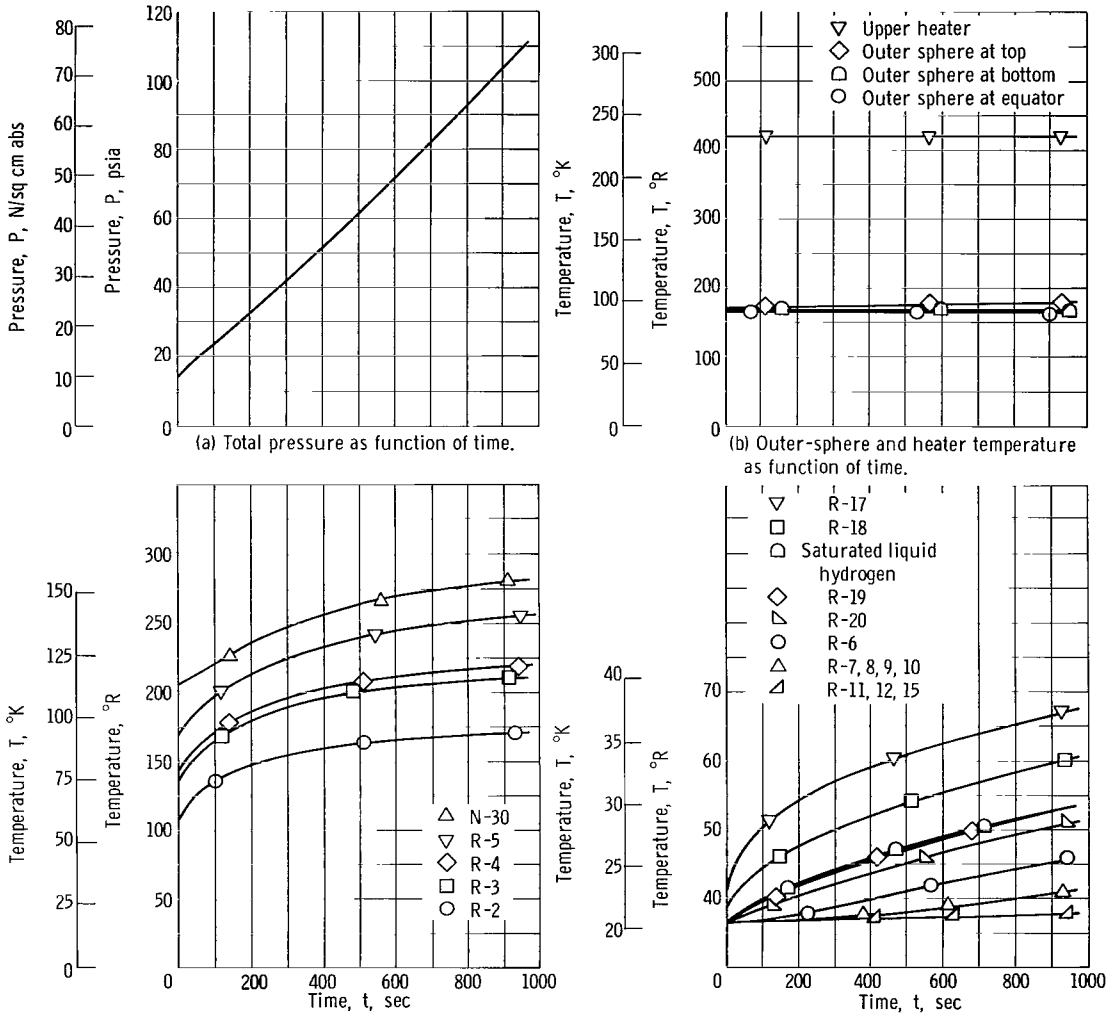

Figure 9. - Test 16. Top heating; initial filling 50.5 percent full; average heat flux, 17.1 Btu per hour per square foot (54 W/m^2). (See fig. 3 for location of transducers.)

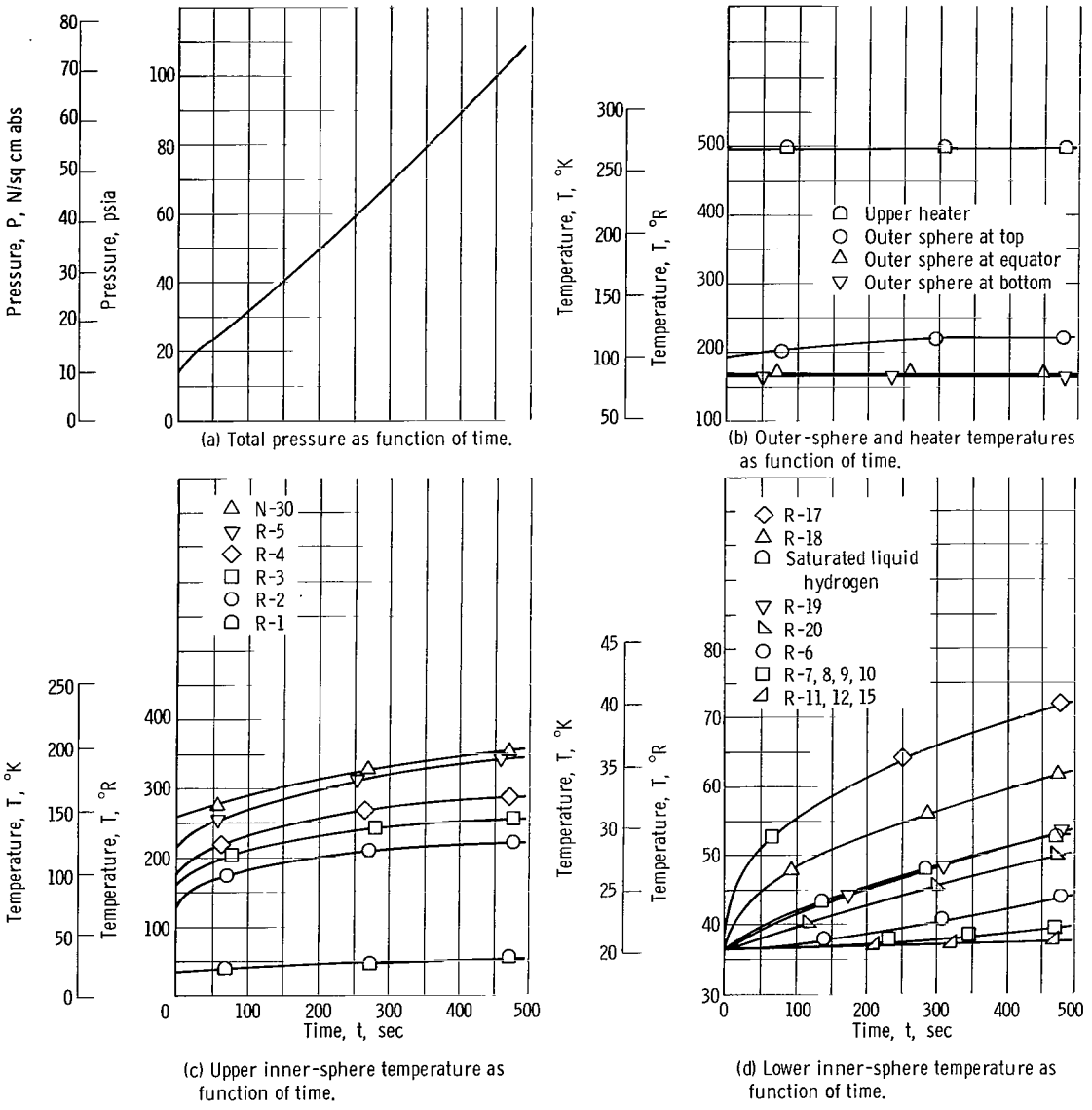

Figure 10. - Test 19. Top heating; initial filling, 51.2 percent; average heat flux, 27.6 Btu per hour per square foot (87 W/sq m). (See fig. 3 for location of transducers.)

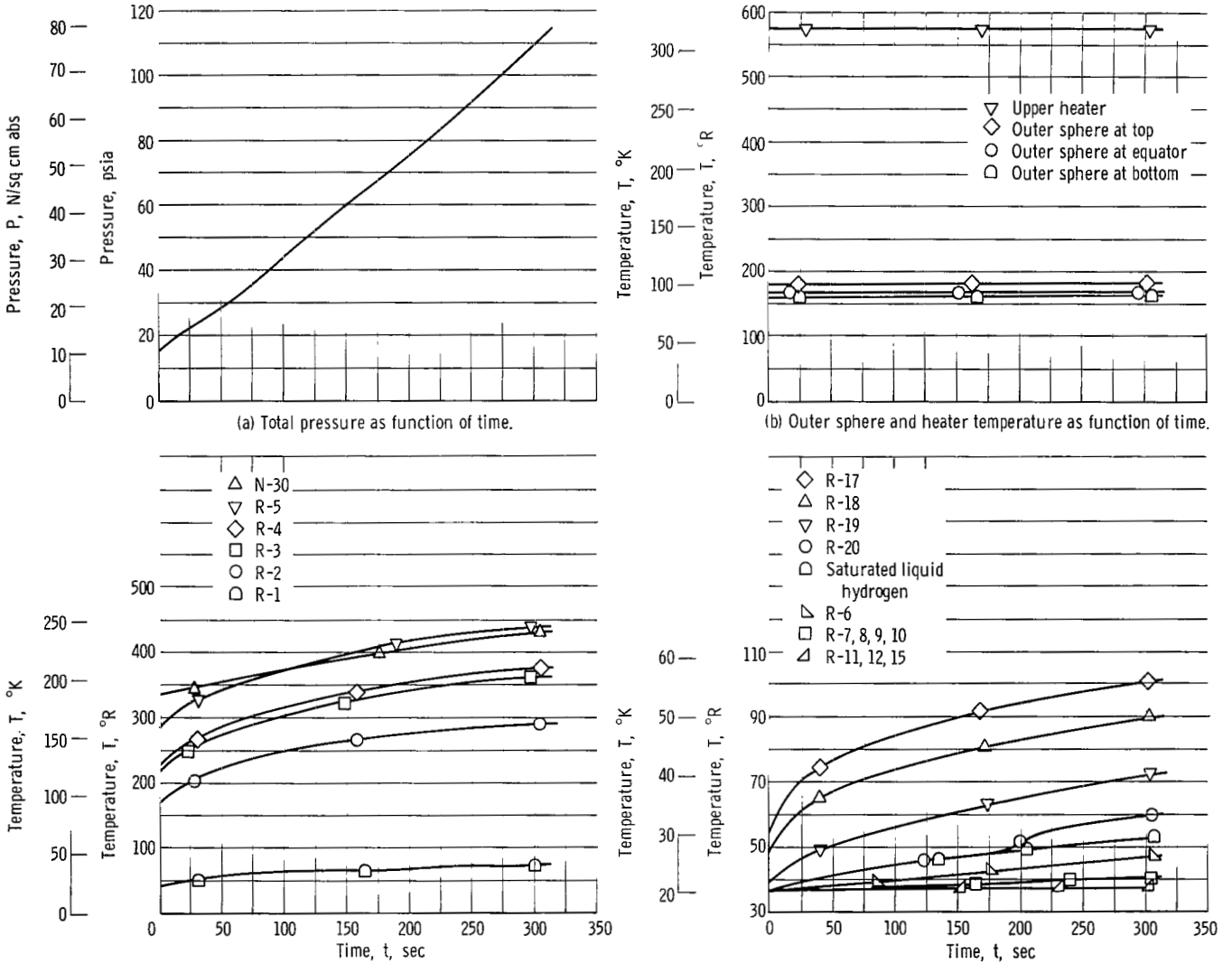

Figure 11. - Test 20. Top heating; initial filling, 47.7 percent; average heat flux, 38.2 Btu per hour per square foot (120 W/sq m). (See fig. 3 for location of transducers.)

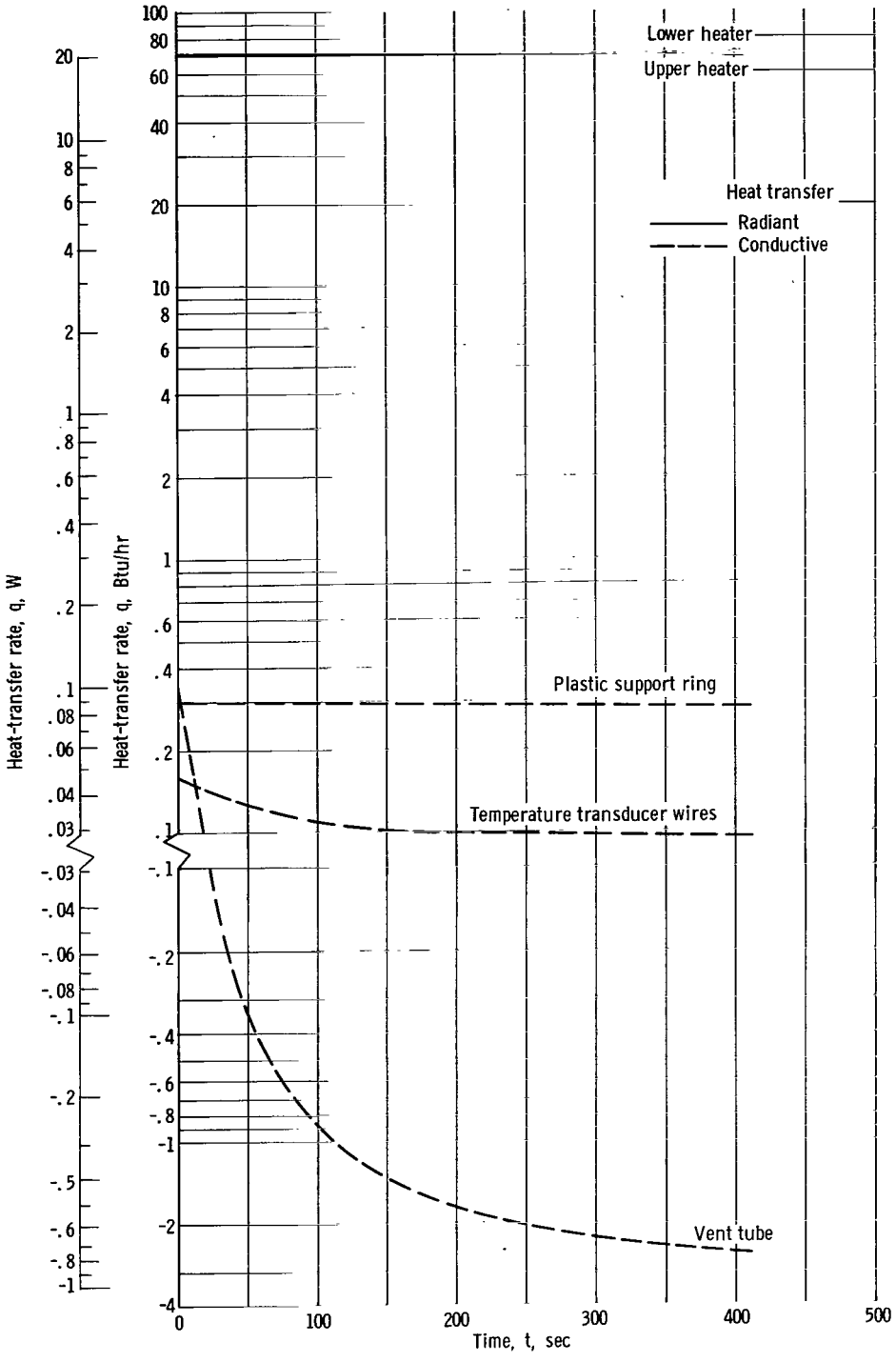

Figure 12. - Rate of heat input as function of time for each heat source for typical quiescent test.

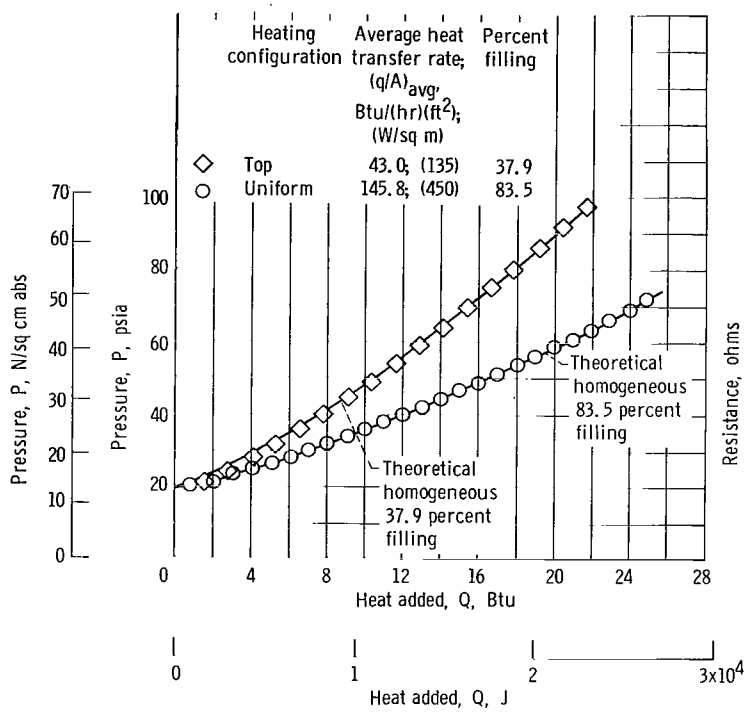

Figure 13. - Pressure as function of total heat added for two homogeneous tests.

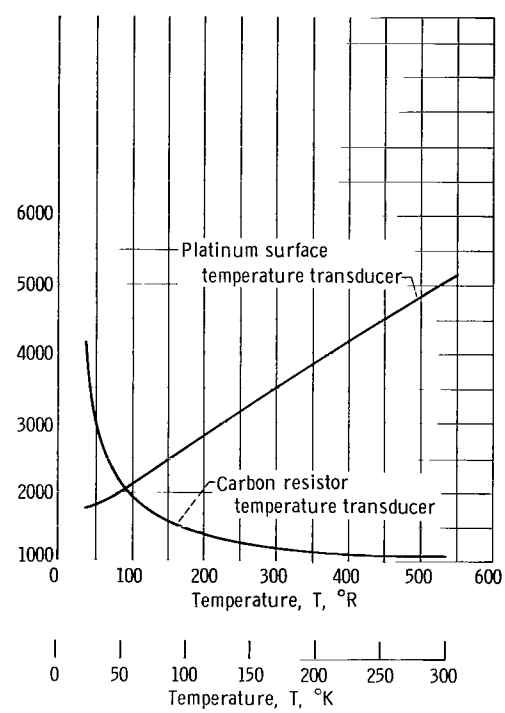

Figure 14. - Resistance as function of temperature for typical inner sphere temperature transducers.

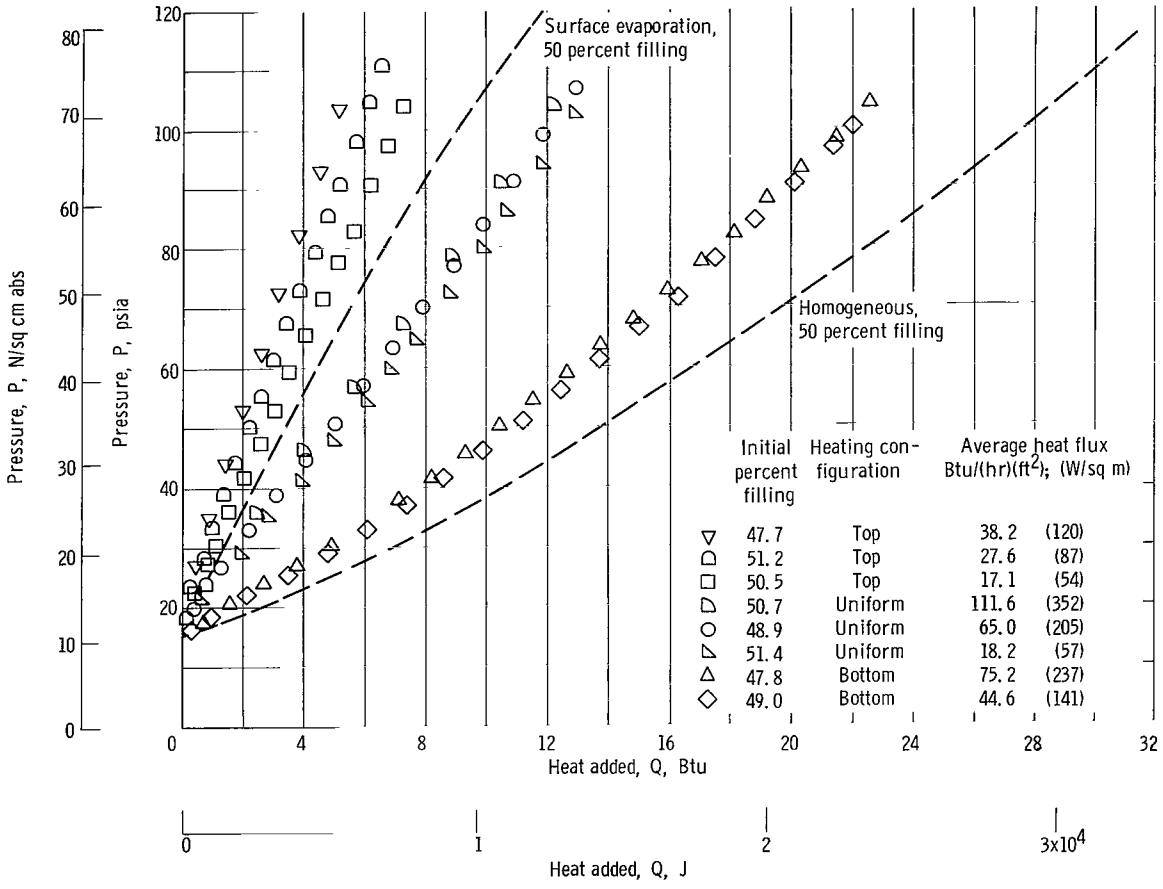

(a) Effect of heat-transfer rate and distribution.

Figure 15. - Pressure as function of total heat added for quiescent tests.

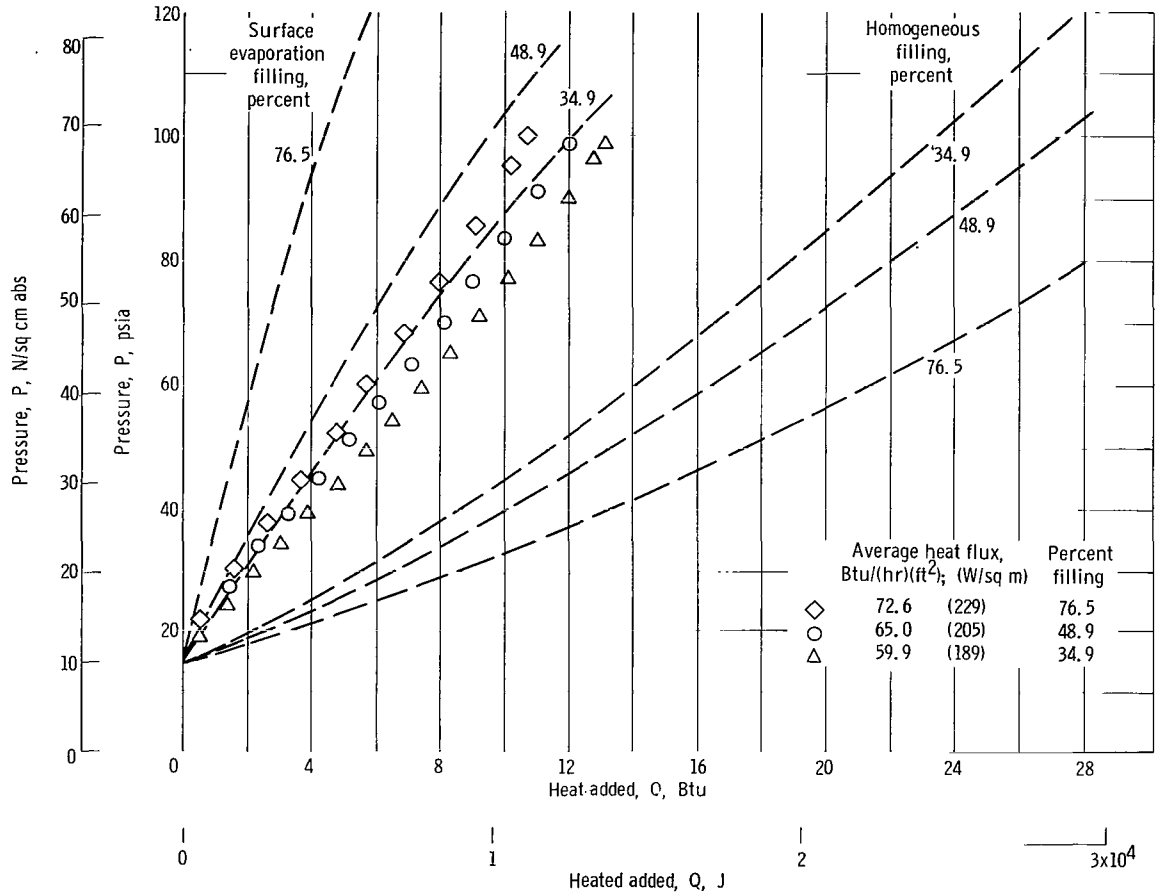

(b) Effect of percent filling.

Figure 15. - Concluded.

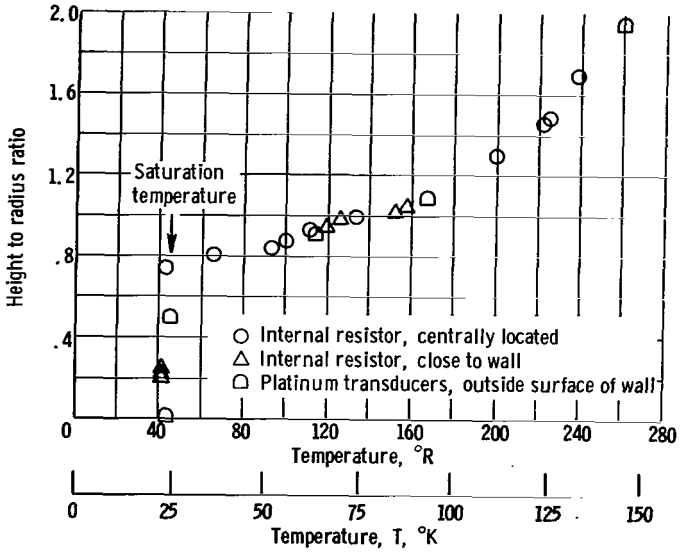

Figure 16. - Inner-sphere temperature as function of position for typical quiescent test. Inner sphere filling, 35 percent.

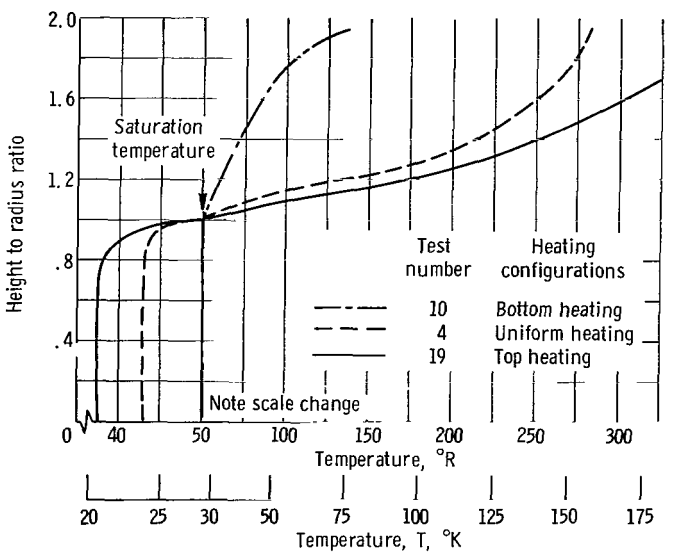

Figure 17. - Inner-sphere temperature as function of position for three heating configurations. Inner-sphere filling, 50 percent.

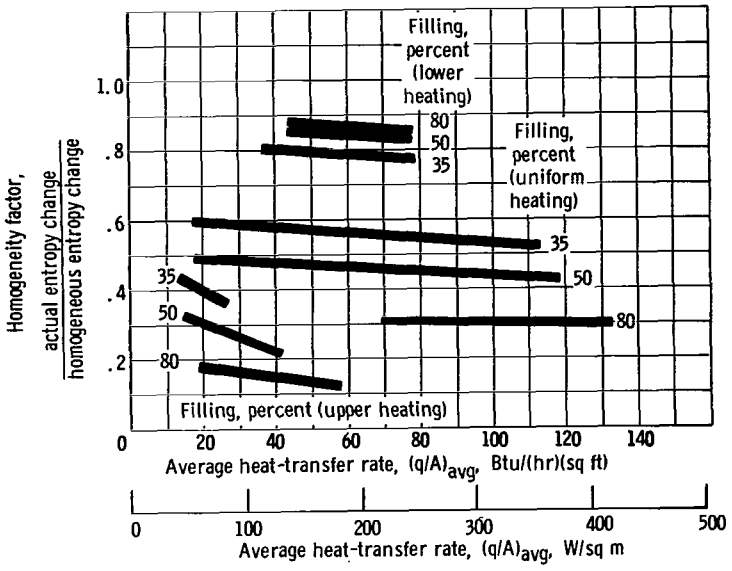

Figure 18. - Homogeneity factor as function of average heat-transfer rate.

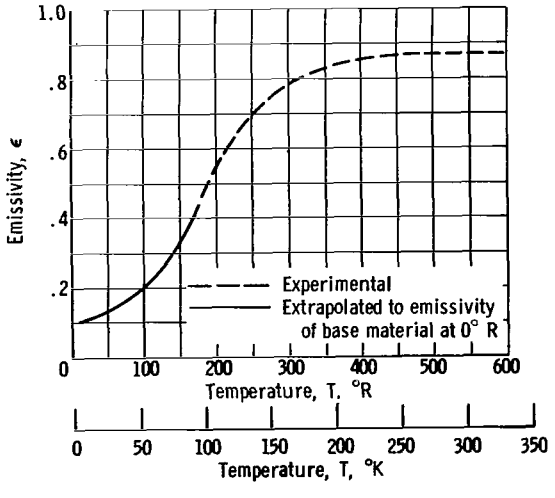

Figure 19. - Inner-sphere and heater emissivity as function of temperature.

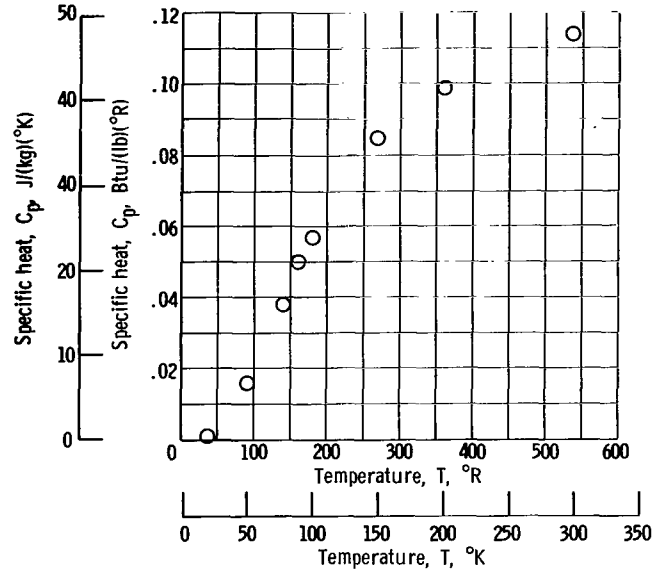

Figure 20. - Stainless-steel specific heat as function of temperature. (Data from ref. 5).

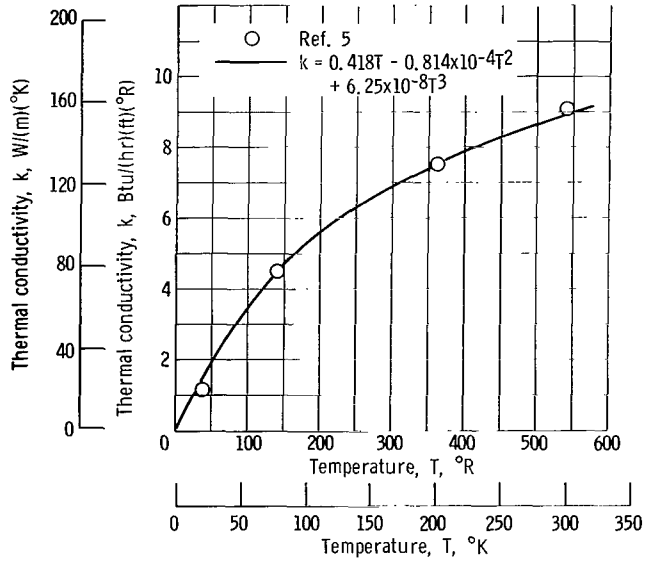

Figure 21. - Stainless-steel thermal conductivity as function of temperature.

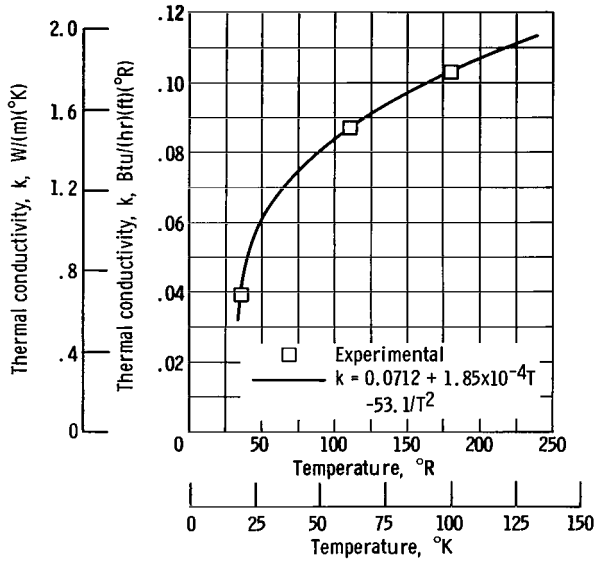

Figure 22. - Plastic support ring thermal conductivity as function of temperature.

"The aeronautical and space activities of the United States shall be conducted so as to contribute . . . to the expansion of human knowledge of phenomena in the atmosphere and space. The Administration shall provide for the widest practicable and appropriate dissemination of information concerning its activities and the results thereof."

—NATIONAL AERONAUTICS AND SPACE ACT OF 1958

NASA SCIENTIFIC AND TECHNICAL PUBLICATIONS

TECHNICAL REPORTS: Scientific and technical information considered important, complete, and a lasting contribution to existing knowledge.

TECHNICAL NOTES: Information less broad in scope but nevertheless of importance as a contribution to existing knowledge.

TECHNICAL MEMORANDUMS: Information receiving limited distribution because of preliminary data, security classification, or other reasons.

CONTRACTOR REPORTS: Scientific and technical information generated under a NASA contract or grant and considered an important contribution to existing knowledge.

TECHNICAL TRANSLATIONS: Information published in a foreign language considered to merit NASA distribution in English.

SPECIAL PUBLICATIONS: Information derived from or of value to NASA activities. Publications include conference proceedings, monographs, data compilations, handbooks, sourcebooks, and special bibliographies.

TECHNOLOGY UTILIZATION PUBLICATIONS: Information on technology used by NASA that may be of particular interest in commercial and other non-aerospace applications. Publications include Tech Briefs, Technology Utilization Reports and Notes, and Technology Surveys.

Details on the availability of these publications may be obtained from:

SCIENTIFIC AND TECHNICAL INFORMATION DIVISION

NATIONAL AERONAUTICS AND SPACE ADMINISTRATION

Washington, D.C. 20546